# Trace-element geochemistry of mantle olivine and application to mantle petrogenesis and geothermobarometry

# Trace-element geochemistry of mantle olivine and application to mantle petrogenesis and geothermobarometry

Jan C. M. De Hoog [a,b,1,✉]

Louise Gall [b,2]

David H. Cornell [b]

[a] Dept. of Earth Sciences, University of Oxford, Parks Road, Oxford OX1 3PR, United Kingdom
[b] Institute of Earth Sciences, University of Gothenburg, Box 460 Göteborg, SE-40530 Sweden

Erratum to article published in
**Chemical Geology**

[1] Present address:
Grant Institute for Earth Sciences, The King's Buildings, University of Edinburgh, West Mains Road, Edinburgh EH9 3JW, United Kingdom
[2] Present address:
Dept. of Earth Sciences, University of Oxford, Parks Road, Oxford OX1 3PR, United Kingdom

✉ Corresponding author. Email: ceesjan.dehoog@ed.ac.uk
Tel: +44-131-650 8525
Fax: +44-131-668 318

**Abstract**

Trace element compositions of olivine from 75 mantle rocks of diverse origin, including xenoliths from kimberlites, basaltic lavas and orogenic peridotites, were determined by laser-ablation ICP-MS to study systematic variations between mantle lithologies, partitioning mechanisms in olivine and the potential of olivine for geothermobarometry and petrogenic mantle processes. Samples were selected to provide a wide range of forsterite contents (89.1-93.4), equilibration temperatures and pressures (750-1450°C; 15-80 kbar).

Trace elements in olivine can be divided into three groups. Group I elements (Ni, Mn, Co, Cu, Zn, Li) show small concentration ranges and olivine is the major host mineral. These are mostly divalent elements and have ionic radii close to that of Mg. Group II elements (Cr, Al, V, Sc, Ca, Na) show large concentration ranges, which are mainly controlled by the equilibration temperature of the host rock. The elements are strongly concentrated in co-existing mantle minerals (garnet, clinopyroxene, spinel) and show a narrow range of bulk rock concentrations. They fit less comfortably in the olivine lattice than Group I elements because of their charge or size. Differences between garnet and spinel-facies rocks are apparent for Al, Ca and Sc. Group III elements (Ti, Zr, Nb, Y) show large ranges of concentration in olivine as well as in co-existing minerals, and are strongly dependent on bulk rock contents. Concentration differences between olivine from garnet and spinel-facies rocks are apparent for all these elements. They are strongly incompatible in olivine and other rock-forming mantle minerals because of their charge or size.

Various mantle lithologies can be discriminated using olivine composition. Spinel, garnet and garnet-spinel peridotites can be distinguished in olivine Sc-Zr and $MnO$-$Al_2O_3$ diagrams, whereas volcanic olivine is distinguished by high Ca and Al contents (picritic olivine) or high Nb contents (kimberlitic olivine). Since concentrations of Group III elements in olivine are diagnostic of whole-rock contents they can be used to trace the petrogenetic history of the

rock. For instance, Ti contents and Cr# (Cr/(Cr+Al)) of olivine correlate with the amount of melt extracted from a mantle residue, although refertilisation may subsequently have increased Ti contents in high-*T* peridotites from the base of the lithosphere.

The olivine dataset can be used to examine substitution reactions. Uptake of Al and Cr appears to be largely charge-balanced by Na in garnet-facies olivine, and olivine Cr# strongly correlates with that of co-existing minerals, in particular clinopyroxene and spinel. In spinel-facies olivine a large excess of trivalent cations is present in olivine, which can be fully attributed to excess Al. This suggests a Tschermak-style substitution, in which replacement of Mg by Al in the octahedral site is charge-balanced by replacement of Si by Al in the tetrahedral site.

Partition coefficients of Group II elements are highly temperature sensitive with most of the element variability being shown by olivine. This allows the definition of simple geothermometers based solely on the concentrations of these elements in olivine. The most widely applicable of these is Al-in-olivine for garnet peridotites, following the expression

$$T_{Al-ol}(^{\circ}C) = \frac{9423 + 53.8P + 1860Cr\#^{ol}}{(13.328 - \ln[\mathrm{Al}]^{ol})} - 273$$

with *P* in kbar, $Al^{Ol}$ the concentration of Al in olivine in ppm, and $Cr\#^{Ol}$ is Cr/(Cr+Al) in olivine. This thermometer predicts the temperature with a residual of 15°C based on calibration with two-pyroxene and Al-in-Opx geothermobarometers (Brey and Kohler, 1990). Although calibrated using lherzolites only, the thermometer performs well for clinopyroxene-free harzburgites and even spinel peridotites. An alternative thermometer is presented for the case where the presence of $Cr^{2+}$ is expected, e.g., for olivine inclusions in diamonds.

The geochemical and thermobarometric information recorded by olivine can be a useful tool in studies of the petrogenesis of lithospheric mantle, olivine xenocrysts in mantle-derived magmas, the formation of diamonds and diamond exploration using detrital olivine.

*Keywords: olivine; peridotite; mantle; geothermobarometry; trace-element partitioning*

## 1. Introduction

Olivine is the most abundant mineral in the upper mantle, as well as a common inclusion in diamond (Sobolev et al., 2008). Despite its abundance, olivine has received relatively little attention in studies of trace-element partitioning and mantle and igneous geochemistry because it contains low concentrations of incompatible trace elements, leading to analytical difficulties. With the advance of analytical techniques many elements can now routinely be determined in olivine, but a framework within which to interpret the results is lacking. This paper presents a comprehensive study of trace element concentrations in mantle olivine from a wide variety of origins and examines the factors that control these concentrations. It explores the viability of olivine geochemistry as a petrogenetic tool and its applicability in geothermobarometry, and establishes olivine trace-element geochemistry as a useful tool for studying igneous and metamorphic processes in the crust and upper mantle. An important potential application lies in fingerprinting olivine xenocrysts, olivine inclusions in diamonds and detrital olivine.

### *1.1. Olivine structure and crystal chemistry*

Olivine is an orthorhombic mineral with continuous solid solution between the two end-members forsterite ($Mg_2SiO_4$; $Fo_{100}$) and fayalite ($Fe_2SiO4$; $Fa_{100}$ or $Fo_0$). In mantle rocks it shows little compositional variability compared to the other rock-forming mantle minerals (garnet, spinel, orthopyroxene, clinopyroxene), with nearly all mantle olivine falling in the range $Fo_{89}$ to $Fo_{94}$ (Deer et al., 1997). Small amounts of MnO and NiO are present at the 0.1-0.4 wt% level, followed by CaO, $Al_2O_3$ and $Cr_2O_3$, other elements generally even lower.

The olivine structure consists of individual $SiO_4$ tetrahedra (T site) linked by six-fold coordinated divalent cations (M sites) (Birle et al., 1968; Burns, 1970). The Si-O tetrahedra point alternatively each way along the *a* axis. The M-site cations occupy two sets of lattice

positions, M1 and M2, both of which are distorted from octahedral symmetry, and M1 being slightly smaller and more distorted than M2 (Birle et al., 1968). Although Fe and Mg are ordered to a high degree, significant disordering may occur for other cations (Lumpkin et al., 1983). Replacement of the main octahedral cations Mg and Fe by other cations is a function of their ionic radius and valence (**Fig. 1**), replacement becoming increasingly difficult with increasing mismatch in size or charge. In addition, several transition metals are influenced by crystal-field effects (Burns et al., 1970).

*1.2. Previous work*

Early trace-element data for mantle olivine determined by ion probe was presented in several comprehensive studies by Hervig et al. (1980a, b, 1986) and Hervig and Smith (1982), who investigated the crystal chemistry of olivine, attempted the use of olivine compositions to make inferences about the origin of cratonic lithosphere, and investigated the applicability of several trace elements as thermometers for garnet and spinel peridotites. They noticed the high Cr contents of diamond inclusions. In their study of the oxidation state of Cr in the mantle, Li et al. (1995) concluded that significant $Cr^{2+}$ may be present in high-*T* (>1600 K) olivine from komatiites and diamond inclusions, but is less important in olivine from lower *T* parageneses. Kurosawa et al. (1997), who measured $H_2O$ and several trace elements (Li, Na, Cr, Al) in mantle olivine, reported a trivalent cation deficiency to charge balance the monovalent cations (including $H^+$) in garnet peridotites, which was attributed to the possible presence of $Fe^{3+}$ (not measured). In contrast, spinel peridotites had an excess of trivalent cations, and they suggested a possible Tschermak-style (MgSi=2Al) substitution in these rocks. Richmond and Brodholt (2000) used atomistic computer simulations to determine the substitution behaviour of $Fe^{3+}$ and concluded that, in the system Si-O-Mg-$Fe^{3+}$, a coupled substitution where ferric iron replaces both Mg and Si is more favourable than vacancy

substitution. Papike et al. (2005) studied the use of olivine as a diagnostic tool for planetary environments with oxidation states different from the terrestrial range, because elements like V, Cr, Fe, and Ti may occur at different oxidation states in those environments, affecting their partitioning behaviour.

Most studies that report trace elements in olivine have dealt with partition coefficients between minerals and their variation with temperature and pressure, with the main focus on spinel peridotites. Pressure-dependence of Ca content in olivine was observed in experiments on a simplified system by Finnerty and Boyd (1978), and was later calibrated using experimental data on natural lherzolite compositions by Köhler and Brey (1990). Unfortunately its use has been hampered by analytical difficulties and the strong temperature dependence of the barometer (O'Reilly et al., 1997). The temperature dependence of Sc and Cr partitioning between olivine and clinopyroxene in spinel peridotites was calibrated by Stosch (1981). O'Reilly et al. (1997) noticed a temperature dependence of Ti and Ca partitioning and observed melting trends in Ni, Mn and Zn. Bodinier et al. (1987) measured pyroxene-olivine partitioning of transition metals including Ti in spinel and garnet peridotites. They observed a pressure dependence of Ti distribution between olivine and orthopyroxene. Partitioning of Ti, Na and REE between spinel peridotite minerals was reported upon by McDonough et al. (1992), who recorded an increased compatibility for HREE compared to LREE in olivine, and clinopyroxene/olivine partition coefficients of 52±8 and 128±23 for Ti and Na, respectively. Eggins et al. (1998) and Bedini and Bodinier (1999) reported partition coefficients for a suite of incompatible trace elements including REE, Zr, Nb, Ta, Ba and Sr in spinel facies peridotites. Concentrations of these elements in olivine were generally <0.1 ppm. A similar study by Garrido et al. (2000) compared laser ablation data with complete digestion analyses of minerals in spinel peridotites from Ronda. They reported that many of the incompatible elements appear to be present in olivine as melt or fluid inclusions. Witt-

Eickschen and O'Neill (2005) studied trace-element partitioning and its temperature dependence in spinel-peridotite minerals, including olivine. They noticed strong temperature dependence of Cr, V, Sc and REE, and suggested the presence of a $MgCrAlO_4$ component in olivine, but did not report Na contents. Recently Wan et al. (2008) calibrated an experimental Al-in-olivine thermometer for spinel-bearing peridotites. Experiments were performed at atmospheric pressure, but the authors noticed that the thermometer gave acceptable results for high-pressure rocks.

The lattice strain model for predicting mineral-melt partitioning (Beattie, 1994; Wood and Blundy, 2003) can be adapted for mineral-mineral partitioning. Even though absolute D values cannot be predicted, relative D values of cations of the same charge can be modelled, and this has been applied to REE partitioning in mantle rocks (Lee et al., 2007; Agranier and Lee, 2007). The application to elements other than REE is unfortunately difficult, as different elements of the same charge may partition into different sites in the minerals in equilibrium with olivine. For instance, Na and Li partition in the M2 and M1 clinopyroxene sites, respectively, as do Zr and Ti, and Al and Cr occupy different sites than REE in all mantle minerals except olivine.

Trace-element partitioning between olivine and melt has been extensively studied, mostly with low-pressure experiments (e.g., Colson et al., 1988; Jurewicz and Watson, 1988; Beattie, 1994; Evans et al., 2008), but also under upper mantle conditions (Taura et al., 1998). Colson et al. (1988) noticed a correlation between partition coefficients and ionic radii, and designed a predictive model for olivine-melt trace element partitioning that took temperature and melt composition into account, a concept that was further developed by Beattie (1994) and subsequently more rigorously by the lattice strain model of Wood and Blundy (2003, see also Bédard, 2005). Colson et al. (1989) argued that REE were charge balanced by vacancies, Cr by tetrahedral Al, and Al by both of these mechanisms, but did not consider monovalent

substitutions. In contrast, Beattie (1994) suggested that REE were charge balanced by coupled substitution with Al for Si, but did not measure Na in olivine. Experimental data in the CMAS system indicated that REE are charge balanced by vacancies, but that Al substitutes into olivine by coupled substitution in octahedral and tetrahedral sites (Evans et al., 2008). Taura et al. (1998) performed experiments at 3-14 GPa to study the high-pressure partitioning between melt and olivine and interpreted partitioning behaviour to reflect a change in Al site distribution from octahedral to tetrahedral with increasing pressure, but also found coupled $Na+M^{3+}$ substitution to be important. Jurewicz and Watson (1988) reported a strong temperature effect on Ca-Mg exchange between olivine and melt, but no discernable pressure effect at P<20 kb. Large variations of $P_2O_5$ concentration, correlated with elevated Al and Cr in otherwise homogenous olivines, have recently been reported in magmatic rocks by Milman-Barris et al., (2008). Similar large P variations have also been observed in otherwise homogeneous mantle minerals by Mallmann et al. (2009).

A few elements have received special interest in the literature, among which are Ti, H and Li. The partitioning of Ti in olivine was studied intensively following the discovery of ilmenite rods in orogenic lherzolites from Alpe Arami, from which a deep mantle origin was inferred (Dobrzhinetskaya et al., 1996). Subsequent experimental work on Ti solubility and partition mechanisms found a strong dependence of Ti partitioning mechanism on water contents, with Ti replacing Si in anhydrous olivine, but replacing Mg as clinohumite defects under hydrous conditions (Risold et al., 2001; Hermann et al., 2005; Berry et al., 2007a). Pressure dependence of Ti solubility in olivine has long remained controversial, with a strong dependence reported by Dobrzhinetskaya et al. (1999) and Tinker and Lesher (2001), yet none by Ulmer et al. (1998). Recent work by Hermann et al. (2005) suggests that no such dependence exists.

The water content of mantle olivine has received considerable interest as well, because of the potentially large influence of water on mantle properties, and since most water in the mantle is hosted by nominally anhydrous minerals (e.g., Kitamura et al., 1987; Bell and Rosman, 1992; Kohlstedt et al., 1996). The current consensus is that the uptake of OH in olivine is related to vacancies related to defect sites, often due to uptake of Ti and trivalent cations (Miller et al., 1987; Matsyuk and Langer, 2004; Berry et al., 2007a, b).

Li has received interest because its isotopes can be used to trace metasomatic and magmatic processes, and olivine is an important Li reservoir in the mantle (Seitz and Woodland, 2000; Kent and Rosman, 2002). Concentrations were found to be at the low-ppm level, although metasomatised peridotites may have slightly higher contents. Partition coefficients were found to be virtually independent of *P*, *T* and mineral composition (Seitz and Woodland, 2000), but may be controlled by phosphorus (Mallmann et al., 2009).

Diffusion is relatively fast in olivine compared to other minerals and therefore in most magmatic rocks zoning is usually limited to late-stage rims. Trace element diffusion has been shown to be fast at magmatic temperatures (Spandler et al., 2007). Dohmen and Chakraborty (2007) pointed out the important effect of trace element site distribution on diffusion, as the incorporation of trace elements may increase the number of vacancies. Diffusion of Al, Cr and especially P are much slower than Fe and Mg, resulting in oscillatory zoning of these elements in many magmatic olivines (Milman-Barris et al., 2008, and references therein) and of P in otherwise homogenous mantle minerals (Mallmann et al., 2009).

## 2. Samples and techniques

### *2.1. Samples*

A total of 75 mantle samples from various localities and lithologies was analysed in the course of this study. Sample locations are listed in **Table 1**. The majority of the samples were mantle xenoliths collected from four kimberlite pipes (Kaalvallei, Premier and Kimberley from South-Africa, Kirkland Lake from Ontario, Canada; dominantly garnet peridotites), an olivine melilitite lava flow (Labait, Tanzania; dominantly garnet peridotites) and an alkaline basalt (Ray Pic, France; dominantly spinel peridotites). In addition, several orogenic peridotites were collected from the Ronda, Spain (spinel peridotites), Otroy Island in Norway, and Pohorje Mountains in Slovenia (both garnet peridotites). Small specimens of the rocks were mounted on glass slides and polished to about 100 µm thickness, apart from samples from Ray Pic, for which mineral separates were mounted in epoxy pucks. Details on the location, petrography and mineral compositions of the samples can be found in **Electronic Appendix 1**. Samples from Ray Pic have been described in detail by Zangana et al. (1997), from Norway by Spengler (2006), and from Pohorje by Janak et al. (2006).

Several Fo-rich olivines from volcanic rocks (picrite, Baffin Island, Canada by Smit et al., 2005; kimberlite, Victor North in Canada by Webb et al., 2004) were analysed for comparison with mantle olivine data. Literature data of spinel peridotites from Germany (Witt-Eickschen and O'Neill, 2005) has been included to augment the data presented in this study.

In this work, samples will be classified based on provenance and lithology. The following lithologies are distinguished: garnet peridotite, garnet-spinel peridotite and spinel peridotite. Occasionally the term garnet-bearing peridotite is used, including both garnet and garnet-spinel peridotites. Likewise, spinel-bearing peridotites include spinel and garnet-spinel peridotites. Garnet-facies and spinel-facies olivine refers to olivine from garnet and spinel-

bearing peridotite, respectively. Furthermore, distinction is made between lherzolites (clinopyroxene-bearing peridotites) and harzburgites (clinopyroxene-free peridotites). Note that the latter definition differs from the common definition of harzburgites as peridotites with 0-5% clinopyroxene. Samples from kimberlites and from Tanzania are referred to as on-craton peridotites, as opposed to those from Ray Pic, France, which are termed off-craton.

*2.2. Analytical methods*

Major elements in olivine (Mg, Fe, Si, Ni, Mn) were analysed by SEM-EDS (Zeiss SEM with Oxford Instruments/LINK EDS system) at the University of Gothenburg (GVC) using 25 kV accelerating voltage, 1 nA beam current, and were quantified using a ZAF algorithm. Signals were calibrated using a Co metal standard and pre-recorded element spectra mainly from pure element and oxide standards. Precision of the forsterite component Mg/(Mg+Fe) was 0.07% based on four repeat analyses of one olivine using 400s live time, whereas it was 0.15% (n=19) using 100s. Therefore, 400s was used for all olivine analyses. Relative precision of MnO and NiO were 20% and 4%, respectively. Accuracy was tested on San Carlos olivine USNM 11312/444, which gave an average Fo value of 90.12±0.07, compared to the certified value of 90.22 (Jarosewich et al., 1980). The compositions of other minerals (garnet, pyroxenes, spinel) were measured using a similar routine with added elements depending on the mineral (Ca, Cr, Na, K, Al, Ti, V, Zn). Results for several reference standards are provided in **Table 2**.

Trace-element concentrations were determined in situ by laser ablation ICP-MS using a Cetac LSX-200 266nm Nd-YAG laser system attached to a HP (now Agilent) 4500 quadrupole ICP-MS at the University of Gothenburg. Spots for laser analysis were selected after careful binocular microscopic examination of the samples to avoid cracks and inclusions in the minerals. The laser spot size was 300µm, or occasionally 200µm if olivines were too

small, and repetition rate was 10Hz. Each analysis consisted of 60s measurement of gas blank and 120s ablation. The following isotopes were measured: $^{7}$Li, $^{23}$Na, $^{27}$Al, $^{29}$Si, $^{31}$P, $^{39}$K, $^{44}$Ca, $^{45}$Sc, $^{49}$Ti, $^{51}$V, $^{53}$Cr, $^{55}$Mn, $^{59}$Co, $^{60}$Ni, $^{65}$Cu, $^{66}$Zn, $^{85}$Rb, $^{88}$Sr, $^{89}$Y, $^{90}$Zr, $^{138}$Ba, $^{140}$Ce and for some samples $^{93}$Nb and $^{43}$Ca. $^{29}$Si was used as internal standard. Signals were carefully monitored for any spikes or an increase in signals of certain elements such as Ba, Rb and Sr which may indicate the presence of cracks or inclusions, in which case the analysis was discarded. To insure minimal matrix effects between runs an in-house olivine standard was prepared from sample DC0212, which had been demonstrated to be homogeneous within uncertainty of laser ablation analysis (<3%) in a reconnaissance study. About 100 grains were handpicked, checked for inclusions by binoculars, washed in dilute $HNO_3$ and mounted in an epoxy puck. Typically four or five olivines of each sample were analyzed, along with two DC0212 grains. Data reduction was performed offline using in-house software (LaserCalc). Reproducibility based on repeat measurements of olivines from DC0212 is 3% or better for most elements, except Na and Zr (both 6%). Rb, Sr, Ba, Ce, Y, K were often near or below detection limits, and only Y contents will be reported here. Detection limits were 0.1 ppm for most elements, except Al, K and Cr: 1 ppm, Na, P and Ca: 5 ppm, and 2-10 ppb for Zr, Y and Nb.

The composition of the DC0212 in-house standard was determined by laser ablation in the Department of Earth Sciences at the University of Oxford using a custom-built New Wave 193nm ArF Excimer laser system attached to a Thermo-Finnegan Element2 magnetic sector ICP-MS in low resolution mode (**Table 3**). In addition to the isotopes analysed at GVC, $^{43}$Ca, $^{63}$Cu and $^{65}$Zn were analysed to quantify potential interfering signals. Ablation took place in He and spot size used was 180 µm. NIST SRM-612 was used for calibration with preferred element concentrations from Pearce et al. (1997), except P from Mallmann et al. (2009).

Olivine grains from sample DC0212 were also analysed by solution ICP-MS after digestion of hand-picked inclusion-free grains in a hot HF-$HNO_3$ mixture, with calibration using olivine-rich dunite reference material NIM-D and with In as internal standard (**Table 3**).

Further accuracy checks of laser ablation analysis were done by analysing the DC0212 standard using a Cameca IMS 4f ionprobe at the School of Geosciences, University of Edinburgh. The epoxy puck with DC0212 olivine grains used for laser ablation analysis was repolished, cleaned by ultrasonication and rinsing with deionised water, and coated with a thin gold layer. Sample spots were sputtered using a 15 nA $^{16}O^-$ beam and an accelerating voltage of 10 kV. Vacuum in the sample chamber was ca. $3x10^{-9}$ mbar, aided by a liquid nitrogen-cooled cold trap, which helped to minimise hydride interferences ($^{26}Mg^1H^+/^{26}Mg^+ < 1x10^{-6}$). Positive ion beam intensities of isotopes $^7$Li, $^{26}$Mg, $^{39}$K, $^{63}$Cu, $^{89}$Y, $^{91}$Zr and $^{93}$Nb were measured at 75V offset at low resolution (R=300), of isotopes $^{24}$Mg, $^{40}$Ca, $^{45}$Sc, $^{51}$V, $^{52}$Cr with 50V offset at medium resolution (R=2200), and of $^{23}$Na, $^{27}$Al, $^{30}$Si, $^{47}$Ti, $^{55}$Mn and $^{59}$Co in both modes. Typical total analysis time (aquired in 6 cycles) for each isotope ranged from 12-120 s dependent on its abundance in olivine and standards. Calibration standards were NIST610 and NIST614 glasses using preferred values from GEOREM (Jochum and Nohl, 2008). $^{30}$Si was used for internal standardisation.

A further interlaboratory comparison of olivine analyses was made by analysing the same grain of San Carlos USNM 11312/444 (Jarosewich et al., 1980) by SIMS (Edinburgh) and laser ablation ICP-MS (GVC and Oxford). The results are in excellent agreement (**Table 3**). A different grain of San Carlos, measured by ion probe in Edinburgh was distinctly different in many trace elements (Na, Al, Sc, Cr, V, Ti, P) to the first grain. This suggests that San Carlos as distributed by the Smithsonian Museum is heterogeneous with respect to several trace elements, which limits its use as a standard for olivine trace-element analysis. However

Ca contents were similar (552 and 563 ppm respectively) and also agree with 524 ppm published by Ottolini (2002).

Potential interferences in olivine from matrix components MgO, $SiO_2$ and FeO, which are generated during ablation only and therefore unaccounted for by gas blank subtraction, were evaluated by comparing signals for different isotopes of various elements to their natural abundance. MgAr interferences (production rate of $^{26}Mg^{40}Ar/\ ^{26}Mg$ ca. was 0.00015%, determined from interference-free $^{67}Zn$) on $^{65}Cu$ and $^{66}Zn$ accounted for 0.1 ppm and 0.2 ppm of the signals, respectively, which is small enough to be ignored for Zn but was subtracted for Cu. SiO interferences (production rate $^{28}Si^{16}O/\ ^{28}Si$ ca. 0.005% determined from interference-free $^{43}Ca$) on $^{44}Ca$ and $^{45}Sc$ are particularly severe for $^{44}Ca$, accounting for 100-150 ppm of the signal. Unfortunately in most samples only $^{44}Ca$ was measured. To correct for the interference its contribution was estimated from the in-house DC0212 olivine standard and subtracted from the sample olivines. The validity of this approach was established on samples in which both $^{43}Ca$ and $^{44}Ca$ were measured; both isotopes resulted in Ca contents within 20 ppm after interference correction of $^{44}Ca$. The contribution of $^{29}Si^{16}O$ to the $^{45}Sc$ signal is about 0.2 ppm, hence a small correction was applied to Sc concentrations.

Matrix interferences from the external reference standard (NIST SRM-612; nominally $SiO_2$, $Na_2O$, CaO and $Al_2O_3$) may influence the accuracy of the measurements. A potential interference of $^{23}Na^{16}O$ on $^{39}K$ could not be evaluated, as both Na and K are monoisotopic. $^{23}Na^{40}Ar$, which may interfere with $^{63}Cu$, was not detected. Therefore, $^{63}Cu$ may be used to avoid the small $^{25}Mg^{40}Ar$ interference on $^{65}Cu$. $^{27}Al^{40}Ar$ (production rate ~0.0065%) produces a significant interference on $^{67}Zn$ of about 12 ppm Zn and its use should be avoided. CaO interferences on $^{59}Co$ and $^{60}Ni$ were undetectable.

Trace elements in various minerals co-existing with olivine (garnet, clinopyroxene, orthopyroxene) were also measured by laser ablation. Analytical procedures were similar to

those for olivine, except that $^{44}Ca$ was used as an internal standard for garnet and clinopyroxene. A spot size of 100µm and a 5Hz ablation rate was used for the latter. Results are presented in **Electronic Appendix 1**.

Modal abundances were determined for one sample suite (Kaalvallei) using a Hitachi SEM equiped with an Oxford Instruments LINK EDS system at GVC, The University of Gothenburg. In a first step, a thousand points were measured on an area of 3.2 $cm^2$ of each thin section using a live time of 2s per point at 15 kV and 3.5 nA beam current. Mineral phases were assigned to each analysis offline (Electronic Appendix 1). Modal data for Ray Pic spinel peridotites were presented in Zangana et al. (1997).

## 3. Results

### *3.1. Mineral compositions*

Averages of mineral compositions for the samples presented in this work can be found in **Electronic Appendix 1**; selected olivine compositions are listed in **Table 3**.

Major-element zoning is nearly absent in most minerals from xenoliths, demonstrating chemical equilibrium in the samples. Where present it is limited to the outer rims of minerals, probably related to heating by the magma that carried the xenoliths to the surface. Orogenic samples (Ronda, Norway, Pohorje) show larger variations in mineral composition, with complex exsolution and replacement patterns in the case of Pohorje (Janak et al., 2006). In xenoliths, exsolution textures were only observed in orthopyroxene from low-*T* garnet and garnet-spinel peridotites, which commonly show rods and laths of chromite and clinopyroxene. All analyses presented here were obtained from the cores of minerals.

*3.2. P-T conditions*

Equilibrium temperatures and pressures for garnet lherzolites (±spinel) were calculated by simultaneously solving the Al-in-Opx and two-pyroxene (2px) geothermobarometers (Brey and Kolher, 1990), except for harzburgites which lack clinopyroxene,in which case the Ca-in-Opx thermometer (Brey and Kolher, 1990) was used. The latter was also used if 2px temperatures were below 800°C, as 2px becomes unreliable at low temperatures due to increasing sensitivity to small variations in CaO content of clinopyroxene (Brey and Kolher, 1990). Both thermometers gave comparable temperatures for the entire sample suite (see **Table 4** for selected samples; *P-T* conditions of the full sample suite are presented in **Electronic Appendix 1**). Temperatures for harzburgites are minimum estimates, as CaO is not buffered by clinopyroxene, but in general they agree well with temperatures calculated by Al-in-Ol thermometry, presented below (Section 4.4.1).

Temperatures for spinel-facies rocks were calculated using the 2px thermometer (Brey and Kolher, 1990) at a constant pressure of 15 kbar for off-craton peridotites and 20 kbar for on-craton peridotites, as no suitable barometer exists for spinel peridotites. Pressures of 12-19 kbar were calculated using the calibration of Mercier et al. (1984), based on the pressure dependence of Ca exchange between orthopyroxene and clinopyroxene, but these calculated pressures showed no correlation with temperature.

Equilibrium *P-T* conditions of the samples are shown in **Fig. 2**. Most cratonic garnet peridotites fall near a 43 $mW/m^2$ conductive geotherm, although many of the deeper samples fall on hotter geotherms. Spinel lherzolites from Ray Pic, France, and Ronda, Spain, plot on a considerably hotter geotherm typical of post-Archean subcontinental lithospheric mantle. The ultrahigh-pressure (UHP) metamorphic garnet peridotites from Norway show a wide range of pressures over a limited temperature interval, which is probably related to disequilibrium in the samples. $Al_2O_3$ content of orthopyroxene, used for pressure estimates, showed

considerable variation among the samples, whereas CaO content, used for temperatures, showed little variation. Because Ca diffusion is likely faster than Al in orthopyroxene, calculated temperatures probably represent UHP metamorphic conditions, whereas Al-based pressures were only partially reset from previous metamorphic episodes.

### *3.3. Trace element contents of olivine*

Three groups of trace elements with distinct behaviour in olivine can be distinguished, and results are presented based on these groups. Selected olivine analyses are presented in **Table 4**; the full dataset can be found in **Electronic Appendix 1**.

#### *3.2.1. Group I elements (Ni, Mn, Co, Cu, Zn, Li)*

Group I elements (**Fig. 3**) show small concentration ranges and olivine is the major host of these elements in mantle peridotites. Group I elements have ionic radii close to that of Mg and are divalent with the exception of Li and possibly Cu (**Fig. 1**). They commonly have relatively high concentrations in other mantle minerals as well, and whole rock concentrations show little variation. Characteristics of each element will be shortly discussed below. The six-fold coordinated ionic radius (after Shannon, 1976) and the most common valency are indicated for each element, as well as its concentration in primitive mantle (PM from McDonough and Sun, 1995; except Cu, Palme and O'Neill, 2007).

*Ni* (0.69 Å, 2+, PM: 1,960 ppm) contents range from 2,040-3,310 ppm and are 2,800 ppm on average. Concentrations increase with Fo content of olivine, and tend to be slightly higher in spinel than in garnet-facies olivine at the same Fo content (ca. 3200 ppm vs. 3000 ppm at $Fo_{92}$; Fig. 3). In typical mantle peridotite, olivine hosts ca. 90% of all Ni. It is the only element besides MgO and Co that has higher concentrations in olivine than primitive mantle

and must therefore be compatible during mantle melting, in accordance with the positive correlation with Fo content.

*Mn* (0.83 Å, 2+, PM: 1,045 ppm) concentrations range from 460 to 850 ppm in garnet peridotites and from 690-1040 ppm in spinel peridotites, and decrease with increasing Fo content of olivine. Lower concentrations in garnet peridotites can be explained by the high affinity of Mn for garnet. About 50% of Mn is hosted by olivine in typical mantle peridotite. In spinel peridotites the highest concentrations are close to PM values.

*Co* (0.65 Å, 2+, PM: 105 ppm) concentrations range from 87-137 ppm and show little systematic variation with Fo content or rock type. Concentrations are on average slightly higher than PM values, while the absence of correlation with Fo indicates a $K_D^{ol/melt}$ very close to one. Olivine contains about 80% of Co in the upper mantle.

*Cu* (0.73 Å, 2+, or 0.77 Å, 1+; PM: 20 ppm) concentrations in garnet peridotites range from 0.4-4.7 ppm, whereas spinel-bearing peridotites show a much narrower range of 1.2-2.0 ppm. Copper contents are very low relative to PM. As co-existing silicate minerals are low in Cu as well (<3 ppm, unpublished data), the low abundance is likely due to the presence of sulfides, for which Cu has a strong affinity. Sulfides were observed in nearly all samples but are strongly corroded. All olivines with Cu content in excess of 2 ppm are from high-*T* peridotites (>1060°C), which suggests a possible *T*-dependence of Cu partitioning between olivine and sulfide, or a change in sulfide phase composition. It is noteworthy that sulfides have a low melting temperature (Bockrath et al., 2004) and are therefore probably molten in high-*T* samples, which may change Cu partition behaviour.

*Zn* (0.74 Å, 2+, PM: 55 ppm) concentrations are rather variable, and behaviour is different in spinel peridotites and garnet peridotites. The latter show a well-defined negative correlation with Fo content (ranging from 28-81 ppm), similar to Mn. The highest values are close to PM, which suggests slightly incompatible behaviour during mantle melting, in agreement with the

negative correlation with Fo content. Spinel peridotites (40-54 ppm) show more scatter and little correlation with Fo content, related to the presence of spinel which has a strong affinity for Zn (O'Reilly et al., 1997). Olivine hosts about 75% of the mantle Zn budget.

*Li* (0.76 Å, 1+, PM: 1.6 ppm) cation size is very close to that of Mg, which explains its preferential partitioning into olivine despite being monovalent. Concentrations range from 0.3-2.45 ppm, and are close to the PM value. There is no concentration difference between spinel and garnet peridotites, but a slightly negative correlation with Fo content can be observed for garnet peridotites. Olivine hosts about 80% of the mantle Li budget.

Subtle differences between mantle olivines and olivines from Fo-rich picrites from Baffin Island and Victor kimberlites can be observed (Fig. 3). MnO is higher in igneous olivines, and in picritic olivines Zn, Co, Cu and Ni are at the high end of mantle values whereas kimberlitic olivines show significant overlap with mantle olivines for these elements.

*3.2.2. Group II elements (Cr, Al, V, Sc, Ca, Na)*

Group II elements show large variations in concentration that are mainly controlled by equilibration temperatures of the olivines (**Fig. 4**). These elements are either main components or strongly concentrated in coexisting mantle minerals (Cr, Al, Sc, V in garnet; Ca, Na in clinopyroxene; Cr, Al, V in spinel). Therefore, the concentrations of these elements are more or less buffered at constant activity in the system. Their contents in olivine are significantly below PM values. Differences between garnet and spinel-facies rocks are apparent for Al, Ca, and Sc. Each element will now be shortly discussed.

*Al* (0.54 Å, 3+ PM: 23,500 ppm) contents vary from 0.6 to 300 ppm. Temperature dependence is very strong, but particularly off-craton spinel-facies olivine has significantly higher concentrations than garnet-facies olivine at the same temperature. Significant differences can be observed for magmatic olivine, with picritic olivine being more Al-rich

(>700 ppm) than any mantle olivine, whereas kimberlitic olivine falls at the low end and mostly has <2 ppm.

*Cr* (0.62 Å, 3+ PM: 2,625 ppm) contents are very similar for spinel and garnet-facies olivine, and range from 23-754 ppm. A strong temperature dependence is observed, but the trend shows significant scatter for spinel and high-*T* garnet peridotites. Picritic olivine has higher Cr values (>475 ppm) than mantle olivine, whereas kimberlitic olivines have low Cr contents (<50 ppm, mostly <20 ppm).

*V* (0.64 Å, 3+, PM: 82 ppm) ranges from 0.9-10.4 ppm and contents are similar for spinel and garnet-facies olivine, although spinel-facies olivines show more scatter. Magmatic olivine values overlap with primitive mantle values.

*Sc* (0.75 Å, 3+ PM: 16.2 ppm) shows a relatively narrow range from 0.4 to 2.6 ppm for garnet-facies olivine and 1.8 to 2.9 ppm for spinel-facies olivine. Both facies show increases with increasing *T*. The clear difference between spinel- and garnet-facies olivine can probably be attributed to the strong affinity of Sc for garnet. Kimberlitic olivine has Sc contents similar to mantle olivine, but picritic olivine values are considerably higher (>4.7 ppm).

*Ca* (1.00 Å, 2+ PM: 25,300 ppm) ranges from 27 to 630 ppm. Concentrations in olivine from off-craton spinel-peridotites are higher than in those from on-craton spinel peridotites and garnet-peridotites. Compared to mantle olivines, picritic olivines show much higher values (2300-2900 ppm) whereas Ca contents of kimberlitic olivines (35-185 ppm) overlap with the lower mantle values.

*Na* (1.02 Å, 1+ PM: 2,670 ppm) behaviour is very similar for spinel and garnet facies rocks, and shows a well-defined trend with temperature. Concentrations range from 3-865 ppm. Magmatic olivine values overlap with the low end of mantle values, but never exceed 150 ppm.

*3.2.3. Group III elements (Ti, Zr, Nb, Y, P)*

Group III elements (**Fig. 5**), apart from P, show the largest variations in concentration, which are mostly controlled by bulk rock contents, as other mineral phases show comparable variations. Differences between garnet and spinel-facies rocks are apparent for all these elements except P.

*Ti* (0.61 Å, 4+ PM: 1,205 ppm) concentrations range from <0.4 up to 290 ppm. A small temperature dependence can be observed, but Ti contents vary over one order of magnitude at given temperature. Concentrations in excess of 30 ppm are almost exclusively observed in garnet-facies olivine, whereas values <2 ppm are typical for olivine from garnet-spinel peridotites. Magmatic olivines overlap with mantle olivines.

*Zr* (0.72 Å, 4+ PM: 10,500 ppb) varies from less than 5 to 440 ppb. Nearly all garnet-facies olivines have concentrations higher than 30 ppb, with exception of olivines from garnet peridotites that also contain spinel, and spinel peridotites nearly all have Zr contents less than 40 ppb. Magmatic olivines overlap with mantle olivines.

*Nb* (0.64 Å, 5+ PM: 658 ppb) range is very large (less than 5 up till 1,100 ppb), with the high values predominantly in garnet-facies olivine. Concentrations in off-craton spinel-facies olivines were all below detection limit (5 ppb) in this study, but data from Witt-Eickschen and O'Neill (2005) indicate a range of 2-20 ppb. Kimberlitic olivine shows high Nb values up to 7,000 ppb, whereas picritic olivine has <5 ppb.

*Y* (0.90 Å, 3+ PM: 4,300 ppb) contents of most garnet-facies olivines fall below detection limit (2 ppb), except for high-*T* olivines, which may contain up to 25 ppb. In contrast, spinel-facies olivines have Y contents up to 62 ppb. Picritic olivines show very high Y contents of >130 ppb, whereas kimberlitic olivine is relatively Y-poor (<30 ppb).

P (0.38 Å, 5+ PM: 95 ppm) shows a relatively small range of concentrations of 5-71 ppm, and are 33 ppm on average. No systematic change with Fo content is observed, although

depleted samples (Fo > 0.92) show a larger range in concentrations. Phosphorus contents of spinel and garnet-bearing peridotites overlap.

## 4. Discussion and applications

### *4.1. Trace element systematics in olivine*

In Section 3 it was shown that trace elements in olivine can be subdivided into three groups with different partition behaviours and temperature dependencies. These differences are further demonstrated in Fig. 6, which shows trace element variations in olivine, clinopyroxene (Fig. 6A) and garnet (Fig. 6B) for representative elements of the three groups (Co, Al and Ti). Concentrations of elements in the various constituent minerals are a function of their concentration in the whole rock (WR), the modal abundance of the minerals and mineral-mineral partition coefficients:

$$C_{WR} = \Sigma_i \, (C_i \, f_i \,) = C_{ol} \, \Sigma_i \, ( \, f_i \, / \, D^{ol/i} \,) \qquad [1]$$

where $C$ is the concentration of a certain element in mineral $i$, and $f$ is the weight fraction of the mineral in the rock. To make the underlying controls more transparent we simplify the system to olivine + clinopyroxene. Taking $C_{cpx} = C_{ol} \, / \, D^{ol/cpx}$, we can write the following equation:

$$C_{WR} = C_{ol} \, f_{ol} + C_{cpx} \, f_{cpx} = C_{ol} \, f_{ol} + C_{ol} \, / \, D^{ol/cpx} \; = C_{ol} \, ( \, f_{ol} + 1 \, / \, D^{ol/cpx} \,) \qquad [2]$$

In the case of Group 1 elements, where $D^{ol/cpx} > 1$, Equation 2 further simplifies to $C_{ol} \approx C_{WR} \, / \, f_{ol}$. This explains the main features of Group 1 elements (Ni, Mn, Co, Cu, Zn, Li), for which olivine is the main host and concentration variations in olivine are small, whereas they can be quite variable in other minerals (Fig. 6). Hence temperature-dependent variations in $D^{ol/cpx}$ have little effect on $C_{ol}$, but a large effect on $C_{cpx}$.

For Group 2 elements (Na, Al, Cr, V, Ca, Sc) the same equations apply, but here $D^{ol/cpx} << 1$. Therefore the opposite is valid: $C_{cpx} \approx C_{WR} / f_{cpx}$, and olivine is very sensitive to variations in $D^{ol/cpx}$ as $C_{ol} = D^{ol/cpx} C_{cpx} \approx D^{ol/cpx} C_{WR} / f_{cpx}$. Most Group 2 elements show considerable variations in whole rock contents, as melting will preferentially dissolve clinopyroxene (the reverse being true for metasomatism) but $C_{cpx}$ and the ratio $C_{WR} / f_{cpx}$ are relatively constant, hence variations of Group 2 elements in olivine are insensitive to bulk rock contents. Thus, variations in $D^{ol/cpx}$ are the main control on $C_{ol}$. It will be demonstrated in Section 4.3 that $T$ is the main control on $D^{ol/cpx}$, hence on $C_{ol}$.

Group 3 elements (Ti, Zr, Nb, REE) are characterised by $D^{ol/cpx} < 1$. However, the variation in $D^{ol/cpx}$ is very small (Fig. 6), whereas the variation in $C_{cpx}$ and thus $C_{ol}$ is largely due to the strong incompatibility of these elements in the main mantle minerals during partial melting. Therefore, Group 3 elements exhibit strong correlations between mantle minerals.

In summary, the differences in trace element behaviour of different groups can be understood based on their mineral/mineral and mineral/melt partition coefficients. Group 1 elements are highly compatible in olivine because of their similarity in size and charge with $Mg^{2+}$, the main cation in olivine. These elements are compatible to slightly incompatible during peridotite melting. Group 2 elements fit less comfortably in the olivine lattice because of their charge and/or size (Fig. 1), whereas they are often major components in co-existing minerals. These elements are moderately incompatible during peridotite melting. Group 3 elements are strongly incompatible in olivine and co-existing minerals because of their charge and/or size, and strongly incompatible during melting.

The systematics discussed above are dependent on the mineral assemblage (garnet vs. spinel peridotites, lherzolites vs. harzburgites). Their use for mantle petrogenesis and thermobarometry will now be discussed further.

*4.2. Olivine as a petrogenetic indicator*

*4.2.1. Lithological information*

Differences in trace-element partition coefficients between olivine and co-existing minerals can be used to distinguish between mantle lithologies. As shown in Section 3.2., many elements show different abundances between garnet and spinel-field olivine because of their different affinities for garnet and spinel (e.g., Mn, Y and Sc partition stronger into garnet than in spinel), or because of pressure dependence of trace-element partitioning. Hervig et al. (1986) successfully distinguished spinel lherzolites from garnet lherzolites in a CaO-$Na_2O$ diagram, but not olivines from low-*T* peridotites and harzburgites. Few elements are characteristic of rocks in which spinel and garnet co-exist. Nevertheless, the three main types of peridotite (garnet-bearing, spinel-bearing, and garnet-spinel bearing) can be successfully distinguished based on Zr and Sc contents of olivine (**Fig. 7a**). Essentially, olivines from garnet peridotites have low Sc but high Zr contents, those from spinel peridotites have high Sc but low Zr contents, whereas those from garnet-spinel peridotites have low contents of both Sc and Zr. This suggests either a strong pressure dependence of Zr partitioning into olivine or increased uptake of Zr in one of the co-existing spinel-field minerals. In-situ analysis of several spinels in the course of this study failed to indicate elevated Zr levels in spinel, and low Zr in spinel was reported by Garrido et al. (2000). We note however, that for equal Zr concentrations in clinopyroxene, spinel-field olivine has much lower Zr than garnet-field olivine, which suggests a compositional control from co-existing clinopyroxene.

An only slightly less successful diagram using elements that can be measured by electron microprobe is $Al_2O_3$ vs. MnO (**Fig. 7b**). It exploits the high affinity of MnO for garnet to distinguish olivine from garnet-bearing peridotites and the temperature sensitivity of $Al_2O_3$ in olivine to distinguish spinel-bearing garnet peridotites, which come from shallow and cooler mantle. Mismatched olivines were predominantly harzburgitic.

No suitable parameter could be derived from the current dataset to distinguish between harzburgites (defined as clinopyroxene absent) and lherzolites. Even though the lack of clinopyroxene indicates that the rocks are Ca-undersaturated, the Ca contents of co-existing minerals (garnet, orthopyroxene) are not significantly lower in harzburgites than lherzolites, except for one sample with subcalcic garnet (A1-P7 from Kirkland Lake). Although it is expected that harzburgites have low concentrations of incompatible elements due to the high degrees of melting they must have experienced, many samples show similar concentrations as lherzolites. This is commonly observed in cratonic peridotites and points to refertilisation of harzburgitic residues by cryptic metasomatism (e.g., Simon et al., 2003).

In addition to various mantle lithologies, magmatic olivines can also be distinguished in the two suites of magmatic olivines analysed in the course of this study. Olivines (>$Fo_{90}$) from picrite basalts are readily distinguished by their high Ca (>2200 ppm), Al (>520 ppm), Cr (>810 ppm), Sc (>4.7 ppm) and Y (>0.13 ppm) contents. In contrast, olivine megacrysts from kimberlites are characterised by extremely low Al (<20 ppm, most <2 ppm), but often relatively high Nb contents (0.03-6.0 ppm, most >0.8 ppm), probably reflecting the bulk chemistry of the kimberlites.

*4.2.2. Melting/fertility indicator*

Trace elements in olivine may provide information about the petrogenetic history of the host rock. In particular Group III elements (Ti, Zr, Y) are suitable, because in the absence of buffering minerals, their concentrations in olivine are strongly dependent on bulk rock concentrations. This is in contrast to Group II elements (Na, Al, Cr) which are too sensitive to temperature to be useful (Fig. 4). For instance, Hermann et al. (2005) showed that, in the presence of a Ti-saturated phase, Ti solubility in forsterite is controlled by temperature, whereas without Ti-saturated phase the dominant control is bulk rock composition. This is also apparent in the data presented here: $TiO_2$ contents of olivine from xenoliths from the

Kaalvallei kimberlite pipe show a strong correlation with whole rock $TiO_2$ contents, as do co-existing minerals (**Fig. 8**). Whole-rock and clinopyroxene $TiO_2$ contents have been applied as melting indicators for residual mantle rocks such as abyssal peridotites and ophiolitic mantle sections (e.g., Bizimis et al., 2000; Niu, 1997) and in abyssal peridotites $TiO_2$ contents correlate strongly with other melting indicators such as $Al_2O_3$ and Yb (e.g., Niu, 2004). Because the $TiO_2$ content of olivine correlates with that of clinopyroxene and whole-rock, it can be used to estimate the degree of melting of residual mantle rocks.

A complicating factor is that partition coefficients between clinopyroxene and olivine are different in garnet and spinel peridotites, as $D_{Ti}^{cpx/ol}$ values are close to 10 and around 110, respectively. No correlations with Fo content or *T* are observed that could explain the difference. Hermann et al. (2005) suggested that the difference is caused by clinopyroxene $Al_2O_3$ contents, based on the exchange reaction $TiAl_2 = MgSi_2$, but no correlation between $D_{Ti}^{cpx/ol}$ and $\#Al^{cpx}$ or $\#Al_T^{cpx}$ is apparent in the data presented here or by Witt-Eickschen and O'Neill (2005). In spinel peridotites $D_{Ti}^{cpx/ol}$ correlates with $\#Mg^{cpx}$, but no such correlation is observed in garnet peridotites. Regardless of the substitution mechanism, olivine Ti contents can be used to estimate whole-rock contents, provided that differences in partition coefficients between garnet and spinel-field olivine are taken into account. It is noteworthy that despite differences in $D_{Ti}^{cpx/ol}$, the relationship between Ti in olivine and whole-rock is very similar in garnet (Kaalvallei) and spinel (Ray Pic) peridotites (Fig. 8). The higher value of $D_{Ti}^{cpx/ol}$ in spinel peridotites is offset by higher Ti contents of clinopyroxene. In spinel peridotites, Ti contents in olivine are expected to decrease from ca. 100 ppm in fertile MORB mantle to about 5 ppm after 25% melting and exhaustion of clinopyroxene from the residue, or even down to 2 ppm during hydrous melting (*cf.* Bizimis et al., 2000). If the melting residues were to be converted into garnet peridotite, e.g., upon deep subduction, Ti contents in olivine would not change significantly (**Fig. 8**), and can therefore be used to estimate the extent of

melting experienced by the protolith. Olivine from garnet-spinel peridotites of this study has Ti contents <1 ppm, indicative of the extreme depletion which these rocks experienced.

To facilitate comparisons of Ti in olivine and clinopyroxene in the literature, which is more commonly used, the following expression can be used (following Fig. 8):

$TiO_2$ Cpx (wt.%) = Ti Ol (ppm) / 180 for spinel-peridotites [3a]

$TiO_2$ Cpx (wt.%) = Ti Ol (ppm) / 510 for garnet-bearing peridotites [3b]

Another element commonly used as a melting indicator is Y, as it behaves similarly to HREE but is about ten times more abundant. A positive correlation can be observed between Ti and Y in olivines from spinel peridotites from Ray Pic. However, no correlation exists with other melting indicators, such as Fo content and Ni in olivine or $TiO_2$ in clinopyroxene. Good correlations between Al, Ti and Y suggest a temperature dependency instead, a feature also observed in spinel peridotites by O'Reilly et al. (1997). Even though bulk rock composition exerts a major influence on olivine $TiO_2$ contents, temperature effects may become visible if bulk rock $TiO_2$ shows little variation. This is the case for Ray Pic peridotites, as clinopyroxene $TiO_2$ contents show a narrow compositional range (0.18-0.43 wt.%). In garnet peridotites no clear correlation between Y and Ti is observed, but Y contents in olivine are strongly influenced by the presence of garnet. It has been proposed that garnet peridotites underwent melting in the spinel facies regime and were later subducted (e.g., Stachel et al., 2004). In such a scenario, the metamorphic growth of garnet after spinel would have strongly depleted the Y contents of the other minerals relative to Ti. Indeed, despite the lack of correlation with Y in olivine, $TiO_2$ in olivine from the Kaalvallei suite correlates rather well with whole-rock Y contents, providing further proof that whole-rock contents of both elements are controlled by melting/refertilisation processes. However Y contents of olivine are strongly modified in the presence of garnet.

An alternative melting indicator potentially applicable to olivine is its chromium number (Cr#, molar ratio Cr/(Cr+Al)). Cr# of olivine is strongly correlated to that of clinopyroxene, orthopyroxene and spinel in all peridotite types (**Fig. 9**). Spinel Cr# in abyssal peridotites correlates with HREE in clinopyroxene and can be used to quantify the extent of melting a rock has experienced (Hellebrand et al., 2001), therefore, the correlation between Cr# in olivine and spinel allows for the degree of melting to be calculated from olivine composition:

$$F_{melting}\ (\%) = 14.5 \times \ln\left( Cr\#^{ol} \right) + 26 \qquad [4]$$

The equation was derived using the analogous equation from Hellebrand et al., (2001) and the linear correlation observed between olivine and spinel Cr# (Fig. 9), which can be represented by $Cr\#^{sp} = 1.2\ Cr\#^{ol} - 0.125$. The two samples from Ronda and one spinel harzburgite (DC0343) from Kimberley were excluded from the calibration. Even though Eq. 4 is strictly speaking only applicable to spinel-bearing peridotites, comparable trends between Cr# of olivine and clinopyroxene in spinel, spinel-garnet as well as garnet peridotites suggest that the presence of garnet and absence of spinel have little influence on Cr# of olivine. Note also that garnet-spinel peridotites fall on the same trend between olivine and spinel Cr# as spinel peridotites.

The calibration by Hellebrand et al. (2001) only applied to samples with spinel Cr# between 0.1 and 0.6 from a fractional melting regime. Batch melting would result in higher melt fractions for the same Cr# compared to fractional melting. At higher spinel Cr# the calibration becomes increasingly unreliable, which is also apparent from the maximum degree of melting in the model which is 26% at Cr# =1. Therefore, the model will need refinement at Cr#>0.6.

Considering the above, a good correlation between $TiO_2$ and Cr# in olivine is to be expected, but is in fact rather poor. A possible explanation is that many garnet lherzolites were refertilised by Ti-rich transient melts, which increased the Ti content of the rocks but

only affected olivine Cr# to a minor degree. Hence, the Ti content of olivine only provides a minimum estimate for the amount of melt extraction a rock has experienced, whereas olivine Cr# may be a more robust melting indicator. It is noteworthy that nearly all high-*T* peridotites (>1150°C) in this study have high Ti in olivine (**Fig. 5**), as it has been proposed that such rocks represent former harzburgites refertilised by astenospheric melts near the base of the lithosphere (*e.g.*, Griffin et al., 1999, 2003).

*4.3. Substitution mechanisms*

Major cations in olivine occur in two valences, 2+ (Mg, Fe) and 4+ (Si), and substitution by cations with equivalent charges ($Ca^{2+}$, $Ni^{2+}$, $Mn^{2+}$, $Cr^{2+}$, $Ti^{4+}$) is straightforward. However, cations with different charges need to be balanced by coupled substitution of other cations, such as $M^{1+} + M^{3+} = 2Mg$, or vacancies, such as $2M^{3+} + [\ ] = 3Mg$.

The elements with the highest abundances in olivine and charges deviating from 2+ or 4+ are $Na^{+}$, $Al^{3+}$, $Cr^{3+}$, and possibly $Fe^{3+}$ and $H^{+}$ (discussed below). In garnet-facies peridotites, the total of structural Na ( $N_{\mathrm{Na}}^{\mathrm{ol}}$ in number of atoms per functional unit of four oxygens) is approximately balanced by Al and Cr ( $N_{\mathrm{Al}}^{\mathrm{ol}} + N_{\mathrm{Cr}}^{\mathrm{ol}}$ ) (**Fig. 10B**). As shown in Section 4.2.2., olivine Cr# in garnet peridotites is strongly correlated with that of pyroxene, whereas there is little correlation with garnet Cr# (Fig. 9). This indicates that the following exchange reaction may take place in garnet-facies olivine:

$$Na(Al,Cr)Si_2O_{6\ (cpx)} + Mg_2SiO_{4\ (ol)} = Na(Al,Cr)SiO_{4\ (ol)} + Mg_2Si_2O_{6\ (cpx)} \quad [5]$$

Even though the Cr# of the exchange is determined by equilibrium with pyroxene, the total uptake of Al, Cr and Na by olivine is determined primarily by temperature (**Fig. 3**; see also Stosch, 1981, and Hervig and Smith, 1982). Therefore, correlations between these elements can be expected even if they are incorporated into olivine by different substitution

mechanisms. The considerable scatter on the Na – Al+Cr diagram (Fig. 10B) indicates that other substitution mechanisms or other cations ($Fe^{3+}$, $H^{+}$, $P^{5+}$) must play a role.

Note that garnet is not a participant in Reaction 5. An exchange reaction with garnet would require the substitution of Cr and Al for Mg and Si in olivine, respectively, which would result in a suprasilicic (majoritic) garnet component and tetrahedral Al in olivine:

$$Mg_3(Al,Cr)_2Si_3O_{12\ (grt)} + Mg_2SiO_{4\ (ol)} = Mg(Al,Cr)_MAl_TO_{4\ (ol)} + Mg_4Si_4O_{12\ (grt)} \quad [6]$$

However, since the total of trivalent cations in garnet-facies olivine is charge-balanced by Na in most garnet peridotites, Reaction 6 appears to be of minor importance. This is further indicated by the poor correlation of olivine Cr# with garnet Cr#. But because majorite becomes stable at pressures over 7 GPa (Rohrbach et al., 2007), higher than most samples from this study, Reaction 6 may increase in importance in olivine from the lowermost upper mantle. Taura et al. (1998) report nearly constant tetrahedral Al, but a strong increase in octahedral Al at the expense of Cr with pressure (3 to 14 GPa), in olivine-melt experiments without garnet present.

In contrast to garnet-facies olivine, a large excess of Al+Cr over Na (in atoms) is observed in spinel-facies peridotites, which can be fully attributed to Al, as Cr contents are similar to garnet-facies olivine. The Al excess can be explained by the uptake of Al following a Tschermak-style substitution, in which replacement of Mg by Al in the octahedral site is charge-balanced by Al replacing Si in the tetrahedral site:

$$MgAl_MAl_TSiO_{6\ (cpx)} + Mg_2SiO_{4\ (ol)} = MgAl_MAl_TO_{4\ (ol)} + Mg_2Si_2O_{6\ (cpx)} \quad [7]$$

The Tschermak component in olivine is isochemical with spinel ($MgAl_2O_4$), which may explain its stability in spinel-facies olivine and its apparent limited importance in garnet-facies olivine. Pyroxenes in spinel-facies peridotites also contain a much larger Tschermak component than pyroxenes in garnet-facies peridotites. The ionic radius of Al is roughly in-between that of Si and Mg (**Fig. 1**), so the substitution of Al for Si is feasible. Witt-Eickschen

and O'Neill (2005) suggested a similar reaction in which uptake of Cr is charge-coupled with Al and proposed the existence of an $MgCrAlO_4$ component in olivine. However, no Na in olivine data was presented in their study, whereas this study shows that Na is abundant enough in spinel-facies olivine to charge-balance all Cr (but not Al) according Reaction 5. It is, however, likely that the following exchange takes place:

$$NaCrSiO_{4\,(ol)} + MgAl_2O_{4\,(ol)} = NaAlSiO_{4\,(ol)} + MgCrAlO_{4\,(ol)} \quad [8]$$

which includes the component suggested by Witt-Eickschen and O'Neill (2005).

In olivine-melt systems a very strong excess of trivalent cations is apparent, which indicates a change in substitution mechanisms. Na contents of olivine phenocrysts from Baffin Island picrites are very low relative to Al and Cr. Similar features can be observed in experimental melt-olivine systems at 1 atm (Wan et al., 2008; Evans et al., 2008). The low Na and high Cr# in the experimental olivines require the presence of significant tetrahedral Al. It appears that the presence of melt strongly decreases Na uptake in olivine. This is supported by experimental data from Borisov et al. (2008), who reported olivine/melt partition coefficients around 0.003, whereas olivine/clinopyroxene partition coefficients in this study range from 0.004 for low-*T* to 0.1 for high-*T* garnet peridotites and from 0.02-0.07 for spinel peridotites.

The presence of $Cr^{2+}$ such as in olivine inclusions in diamond and komatiite olivine, which can have large excess Cr (Pyke et al., 1975; Hervig et al., 1980a) would affect the Cr substitution mechanism. However, temperatures in excess of 1400°C are needed to stabilise significant $Cr^{2+}$ at common mantle oxidation states (Li et al., 1995), which is at the upper temperature limit of xenoliths in this study.

A complicating factor in resolving substitution mechanisms is the possible presence of $Fe^{3+}$ and water, which have not been measured in this study. Even though a $Fe^{3+}$ end-member of fayalite exists (laihunite, $Fe^{2+}Fe^{3+}{}_2(SiO_4)_2$; Dyar et al., 1998), the ferric iron content of natural mantle olivine is generally regarded as negligible (Dyar et al., 1989; Canil and

O'Neill, 1996). However, due to the low trivalent cation content of olivine, a small excess of ferric iron may have a significant effect on trace element charge-balancing reactions. A ferric iron content of several hundreds of ppm was predicted by Dohmen and Chakraborty (2007). The authors noted an increase of trivalent iron on the Si site at higher temperatures, so ferric iron becomes self-neutralising following the reaction $MgSi=2Fe^{3+}$.

The influence of water is difficult to evaluate. Using FTIR spectroscopy it has been demonstrated that water is present in natural mantle olivine as Ti-clinohumite point defects (Berry et al., 2005, 2007a, b), and the uptake of $H_2O$ by olivine appears to be charge neutral. In that case the influence of water on the substitution reactions discussed above is likely to be minimal.

Lastly, fluorine may play a role in the uptake of trivalent cations according the reaction $Mg_2SiO_4 = Mg_2AlFO_3$, but recent work suggests that fluorine concentrations in peridotitic olivine are generally less than 10 ppm (Guggino et al., 2007), and therefore insignificant relative to the contributions of other charge-balancing elements.

*4.3.2. Other cations*

The partitioning of Ti in olivine has recently received much attention as it is thought to be instrumental in the incorporation of water in olivine, with important implications for the geophysical properties of the mantle (Berry et al., 2005, 2007a, b). Experimental data shows that Ti occupies the tetrahedral (Si) site under anhydrous conditions ($Mg_2Ti_TO_4$), but changes to six-fold coordination when water is present, forming clinohumite $MgTi_M[\ ]O_2(OH)_2$ defects associated with a Si vacancy (Berry et al., 2007a). No correlation of Ti with other elements is observed in this study, in agreement with both experimental exchange mechanisms, as the amount of Ti is too small to show any significant decrease in Si. Titanium solubility experiments by Hermann et al. (2005) indicate that the expected upper limit in anhydrous mantle rocks is about 350 ppm $TiO_2$ (equivalent to 210 ppm Ti). Titanium contents

of many olivines from this study exceed the theoretical solubility of the $Mg_2TiO_4$ component in olivine (the maximum observed in this study is 290 ppm Ti), which points to significant amounts of the Ti-clinohumite point defect (Hermann et al., 2005; Berry et al., 2007a) and the possible presence of several hundreds of ppm dissolved $H_2O$.

An additional component in olivine is $P_2O_5$, which may reach high concentrations up to 0.4 wt% in magmatic olivine (Milman-Barris et al., 2008), and is probably incorporated in olivine via vacancy substitution mechanisms, possibly involving Al and Cr (Boesenberg et al., 2004; Milman-Barris et al., 2008; Mallmann et al,. 2009). The majority of olivines in the current study contain 15-60 ppm P, which potentially has a significant charge-balancing effect. Since no correlation exists with any of the other elements measured in this study, the role of P in mantle olivine remains unclear, but the results are consistent with the proposed vacancy substitutions observed at low *P* and high *T* (Boesenberg et al., 2004).

*4.4. Calibration of empirical olivine thermobarometers for garnet peridotites*

The distribution of an element *i* between two minerals $x_1$ and $x_2$ can be expressed as:

$$\ln D_i^{x1/x2} = a + (b - P)/T \text{, where } D_i^{x1/x2} = C_i^{x1} / C_i^{x2} \quad [9]$$

If the variation in concentration of element *i* in one of the minerals is negligible compared to the variation in the other mineral, the equation simplifies to:

$$\ln C_i^{x1} = c + (b - P)/T \text{, where } c = \ln C_i^{x2} + a \quad [10]$$

This formulation can be used to define single-mineral geothermobarometers that can be applied to, e.g., olivine inclusions in diamonds, olivine xenocrysts and detrital olivine. In order to demonstrate that variations in trace elements are mainly determined by temperature (and to some extent pressure), we calculated olivine-mineral partition coefficients for Group 2

elements using multiple linear regression (**Table 5**). Strong temperature correlations confirm the temperature-sensitive nature of these elements and are presented graphically in **Fig. 11**. Fits for $D^{ol/cpx}$ improved slightly when $\#Na_{cpx}$ was incorporated as a parameter. Titanium was included to demonstrate that Group 3 elements show little correlation with temperature and cannot be used for geothermometry, but may provide information about bulk rock composition instead (Section 4.2.2.). Cobalt was included to show that Group 1 elements are temperature sensitive as well, but since olivine is the main host, the variation is mostly due to Co variation in clinopyroxene. It can therefore not be used as a single element thermometer for olivine, but could be used for clinopyroxene instead.

Calibration of trace-element based geothermobarometers was performed on a subset including all garnet lherzolite xenoliths from the dataset presented in this paper, with the exception of three xenoliths that exhibited mosaic textures which gave strongly anomalous results. The geothermobarometers were calibrated by solving the parameters *a*, *b*, *c*, and *d* for the equation:

$$T = (a + bX + cP) / (\ln C_i^{ol} - d) \quad [11]$$

by minimising $\Sigma(T_{2Px} - T_{calculated})^2$. *X* represents a compositional parameter such as $Cr\#^{ol}$. Values for *P* and *T* were calculated from 2px thermometer and Al-in-opx barometer (Brey and Kohler, 1990) for garnet lherzolites and Ca-in-opx thermometer for garnet harzburgites (see Section 3.1 for details).

Even though the equation is a simplification which ignores compositional variations in co-existing minerals, we chose this approach to increase the applicability of the geothermobarometers. In addition, we found that the influence of compositional parameters was limited or can be successfully approximated by olivine compositions, such as $Cr\#^{ol}$ which closely resembles $Cr\#^{cpx}$. Evaluation of the performance of the thermobarometers was done

including the aforementioned garnet lherzolites, seven garnet harzburgites and six garnet-spinel lherzolites. The latter two categories were not included in the calibrations to avoid potential bias due to differences in the equilibrium mineral assemblages. The focus here is on geothermobarometry of olivine in garnet peridotites, because spinel peridotites have been extensively studied in the literature previously (e.g., O'Reilly et al., 1997; Witt-Eickschen and O'Neill, 2005). However, accurate performance for spinel field olivine could increase the applicability of the thermobarometers and will therefore also be evaluated.

*4.4.1. Al-in-olivine*

The most promising thermometer is Al-in-olivine for garnet peridotites, following the expression:

$$T_{Al-ol}(^{\circ}C) = \frac{9423 + 51.4P + 1860Cr\#^{ol}}{(13.409 - \ln[\mathrm{Al}]^{ol})} - 273 \qquad [12]$$

where $[Al]^{ol}$ is the Al content of olivine in ppm, and $Cr\#^{ol}$ is Cr/(Cr + Al) of olivine. The thermometer is presented graphically in Fig. 12A. The parameter $Cr\#^{ol}$ was introduced to take into account the Al activity of the system. If *P* is unknown, it is advisable to make use of the *P*-*T* correlation of the geotherm from the sample location (e.g., ca. 42 mW/m$^2$ conductive geotherm in many cratonic areas).

The average deviation of $T_{Al\text{-}ol}$ ($\Delta T$) from the calibration temperatures is 15°C (Fig. 12B). The equation is also reasonably successful in predicting pressures, as the average deviation from the calibration pressure ($\Delta P$) is 2.8 kbar. However, the strong temperature dependence (about 1.9 kbar per 10$^o$C) prohibits its successful use as a geobarometer unless equilibration temperatures are accurately known (e.g., in experimental data).

Calculated *T* for harzburgites (which were not included in the calibration) are in excellent agreement with the CaO-in-Opx thermometer from Brey and Kohler (1990) (Fig. 12B) even though, in the absence of clinopyroxene, this thermometer provides a minimum *T* estimate

only. An exception is one harzburgite that contains subcalcic garnet (sample A1-P7). Here $T_{\text{Al-ol}}$ is 111°C higher than $T_{\text{CaO-opx}}$, but probably more accurate, as it is not dependent on the presence of clinopyroxene. This is relevant to the study of olivine inclusions in diamonds, as these are often of harzburgitic origin, so Al-ol thermometry may give an accurate estimate of the temperature at which the diamond formed, provided *P* can be estimated independently.

Calculated temperatures for olivines from garnet-spinel lherzolites are in excellent agreement with calibration temperatures as well (Fig.12B), hence the thermometer can also be applied successfully to this rock type. Strictly speaking, the thermobarometer applies only to garnet-bearing rocks, but the thermometer also predicts equilibrium temperatures in spinel peridotites rather well, although the results are more scattered than for garnet peridotites (average *T* difference: 29°C). This may seem surprising, considering the excess Al due to the presence of tetrahedral Al, however co-existing pyroxene in the spinel stability field also has a high Tschermak component.

Olivine from mosaic-textured peridotites always gives much too high Al-ol temperatures. As these samples experienced dynamic recrystallisation under shear stress, it appears that this process caused disequilibrium in trace-element contents of recrystallised olivines.

Garnet peridotites from Norway show a range in equilibration temperatures, even though Al contents of olivine fall within a narrow range (5.0-5.5 ppm). The temperature variation appears to be an artefact of the variability of $Al_2O_3$ in Opx, which results in a wide range of calculated equilibration pressures. At a fixed pressure of 35 kbar, $T_{\text{Al-ol}}$ falls in a narrow range of 784-798°C, which is slightly higher than $T_{\text{Ca-opx}}$ (711-763°C) at the same *P*. Orthopyroxene possibly records Al contents from an earlier higher-pressure stage, as microdiamonds in surrounding crustal rocks indicate subduction to greater pressures (Dobrzhinetskaya et al., 1995). One garnet peridotite from Pohorje records a very low $T_{\text{Al-ol}}$ of 591°C at 21 kbar ($P_{\text{BK90:Al-Opx}}$); much lower than conventional geothermometry (ca. 900°C at 40 kbar; Janak et

al., 2006). Possibly the olivine re-equilibrated along the exhumation path, whereas conventional geothermobarometry retrieved peak *P-T* information from the cores of partially retrogressed minerals (Janak et al., 2006).

The Al content of olivine has previously been used to calibrate a barometer in an unpublished dataset (PTMLR.XLS) based on experiments by Brey and Kohler (1990) and Kohler and Brey (1990). The equation can be rewritten to be used as a thermometer using $\ln D_{Al}^{Ol/Grt}$, and when applied to our dataset, results in temperatures about 30°C higher than the calibration presented in this study, with comparable pressure dependence. The temperature offset is likely related to inter-laboratory differences, but in fact the results show a remarkable correlation between experimental results and natural samples, which attests to the robust nature of Al-ol thermobarometry.

Equation 12 requires the Cr content of the olivine to be measured in addition to Al, and assumes Cr to be present as $Cr^{3+}$. If Cr cannot be measured, or when the presence of $Cr^{2+}$ can be expected, such as in diamond inclusions (Hervig et al. 1980; Li et al., 1995), the following simplified formula can be used:

$$T_{Al-ol}(^{\circ}C) = \frac{11959 + 55.6P}{(14.530 - \ln[\mathrm{Al}]^{ol})} - 273 \qquad [13]$$

with *P* in kbar and $[Al]^{ol}$ the Al content of olivine in ppm. As can be expected, the thermometer perform less well because of ignoring Cr#, but the average deviation of calculated *T* from the calibration *T* is still only 20°C. The calibration is valid for olivine Cr# of 0.35 to 0.75, which translates to Cr# of 0.15-0.45 in clinopyroxene. It performs equally well for harzburgites and spinel-garnet peridotites, however, results for spinel peridotites show larger scatter (ca. 60°C).

*4.4.2. Cr-in-olivine*

Chromium in olivine behaves very similarly to Al, and its temperature dependence can be expressed by:

$$T_{Cr-ol}(^{\circ}C) = \frac{13444 + 48.5P - 4678Cr\#^{ol}}{(14.53 - \ln[\mathrm{Cr}]^{ol})} - 273 \qquad [14]$$

where $Cr\#^{ol}$ is Cr/(Al + Cr) in atoms and $[Cr]^{ol}$ is the Cr content of olivine in ppm. The pressure dependence of this thermometer is similar to that of the Al thermometer. On average it reproduces *T* within 15°C and *P* within 2.9 kbar. Using $K_D$(NaCr) following Hervig et al. (1986) does not lead to an improved fit for this sample suite. Unlike the Al-ol thermometer, an expression without $Cr\#^{Ol}$ leads to significantly worse *T* estimates. Note that Al-ol is the preferred geothermometer, but significant deviation of $T_{Cr\text{-}Ol}$ may indicate the presence of $Cr^{2+}$ or disequilibrium.

Results for olivines from harzburgites agree well with calibration temperatures, whereas garnet-spinel peridotites show an offset of 25°C to lower temperatures, which slightly exceeds the uncertainty in the calibration. Results for spinel lherzolites are more scattered than for garnet peridotites but with little bias (4°C) for Ray Pic xenoliths. However, the thermometer is less accurate for the low-*T* samples from Witt-Eickschen and O'Neill (2005). We notice however, that discrepancies of up to 100°C, exist between the two thermometers presented in Witt-Eickschen and O'Neill (2005). If we compare our results with $T_{(2px;\ BK90)}$ from their study, instead of $T_{(Ca\text{-}Opx:\ BK90)}$, the fit is much better, with the average deviation from the measured *T* being 29°C. Nevertheless, significant scatter is observed in the predicted temperatures, hence caution is needed when applying the Cr-Ol thermometer to spinel peridotites.

*4.4.3 Ca in olivine*

The calcium content of olivine can be calibrated as a thermometer with the expression:

$$T_{Ca-Ol}(^{\circ}C) = \frac{10539 + 79.8P}{(15.45 - \ln Ca^{Ol})} - 273 \quad [15]$$

where $Ca^{Ol}$ is the Ca content of olivine in ppm and with $P$ in kbar. Results are less good than for the geothermobarometers involving Al and Cr ($\Delta T$=30°C, $\Delta P$=3.9 kbar), and are probably negatively influenced by uncertainties in Ca contents of olivine due to the correction for $^{28}Si^{16}O$ interference (see Section 2.2). Harzburgites are slightly offset to lower $T$ by 32°C, which may be due to the absence of clinopyroxene in the assemblage, but garnet-spinel peridotites show very little bias (4°C). Results for spinel lherzolites are excellent (slightly offset to higher $T$ by 11°C), which is encouraging because Ca partitioning behaviour is expected to be similar in garnet and spinel peridotites.

Calcium distribution between clinopyroxene and olivine has been calibrated as a geobarometer by Kohler and Brey (1990). The data presented here can be calibrated using a similar equation:

$$T_{Ca-Ol}(^{\circ}C) = \frac{7335 + 66.9P}{(1.60 - \ln D_{Ca}^{Ol/Cpx})} - 273 \quad [16]$$

where $D_{Ca}$ = $\#Ca^{Ol}/\#Ca^{Cpx}$ with #Ca as the number of Ca cations in the structural formulae of olivine and clinopyroxene based on 4 and 6 oxygens, respectively, and with $P$ in kbar. The calibration performs similarly to Equation 15, with $\Delta T$=34°C and $\Delta P$=3.8 kbar. However, a significant offset is observed between the Kohler and Brey (1990) calibration and that presented here. This could be due to inter-laboratory differences in Ca measurements, but also to non-linearity in the calibration of Ca-based geothermobarometers. Kohler and Brey (1990) needed to invoke two different equations at high and low temperatures, respectively, to obtain a reliable geobarometer. Nearly all samples here fall in the low-$T$ version of their calibration, but a much better correlation is obtained with their high-$T$ version, albeit still significantly offset. Different authors have reported variable success using Ca-Ol barometry (e.g., O'Reilly

et al., 1997) and more work is needed to fully understand the idiosyncrasies of the *P* and *T* dependence of Ca partitioning in natural mantle samples.

*4.4.4. Na in olivine*

Sodium in olivine has potential to be a useful geothermometer, because Na, unlike Al-Ol and Cr-Ol thermometers, will be independent of Cr# of co-existing minerals. Also it neither has a variable oxidation state like Cr, nor changes site distribution between tetrahedral and octahedral sites like Al. However, a thermometer derived from the current dataset performs considerably worse than the Al-Ol and Cr-Ol thermometers presented above. Using $D_{Na}^{Ol/Cpx}$ instead of the Na concentration of olivine improves the result only slightly.Therefore the high uncertainty is probably due to the relatively high analytical uncertainty in the determination of Na in low-*T* samples, because of high Na backgrounds during ICP-MS analysis.

## 5. Conclusions

Trace elements in olivine can be divided into three groups: Group I elements (Ni, Mn, Co, Cu, Zn, Li) show a narrow range of concentrations and olivine is their major host mineral. They are mostly divalent elements with ionic radii close to that of Mg and often show correlations with Fo content. Group II elements (Cr, Al, V, Sc, Ca, Na) show a large range in concentrations, controlled mainly by the equilibration temperature of the rock. They fit less comfortably in the olivine lattice than Group I elements because of their charge or size, and are strongly concentrated in co-existing mantle minerals. Group III elements (Ti, Zr, Nb, Y, P) show the largest ranges of concentrations in olivine, which are mostly controlled by bulk rock contents. They are strongly incompatible in olivine as well as co-existing rock-forming mantle minerals because of their charge and/or size.

The incorporation of monovalent and trivalent trace elements occurs following two principle substitution mechanisms: $M^{1+}M^{3+} = 2Mg$ and $M^{3+}Al^{3+} = MgSi$. The first reaction is dominant in all peridotites, but the second reaction accounts for a significant proportion of Al uptake in spinel peridotites, and may be dominant in magmatic olivine. Olivine Cr# is strongly correlated with those of co-existing pyroxenes and spinel.

Differences between mineral-olivine partition coefficients for various minerals can be used to determine the lithology from which olivine was derived. For instance, garnet, garnet-spinel and spinel peridotites can be successfully distinguished in Zr-Sc space and less successfully, in MnO-$Al_2O_3$ space. $TiO_2$ contents and Cr# of olivines can be used to reconstruct petrogenetic processes such as melting and metasomatic history. The temperature dependence of Group II elements can be used to derive sensitive geothermometers, of which Al-in-ol is the most generally applicable, as it can be successfully applied to garnet-bearing peridotites including clinopyroxene-free lithologies.

**Acknowledgements**

The authors gratefully acknowledge Dan Schulze (U. of Toronto), Hilary Downes (London College), Gareth Davies and Melanie Morel (Vrije Universiteit, Amsterdam), Dirk Spengler (University of Utrecht) and Mirijam Vrabec (University of Ljubljana) for providing samples from their collections, and De Beers Consolidated Mines for permission to collect at the Kimberley pool mine dumps. Detailed reviews by Cin-Ty Lee and especially Hugh O'Neill significantly improved the clarity and consistency of the manuscript, while Roberta Rudnick is thanked for editorial handling. JDH wants to thank John Craven and Richard Hinton on advice how (not) to use the ion microprobe. This research was partially funded by Vetenskapsrådet (Swedish Research Council) grant nr. 621-2002-4282.

**References**

Agranier, A., Lee, C.-T.A., 2007. Quantifying trace element disequilibria in mantle xenoliths and abyssal peridotites. Earth and Planetary Science Letters 257, 290-298.

Beattie, P., 1994. Systematics and energetics of trace element partitioning between olivine and silicate melts; implications for the nature of mineral-melt partitioning. Chemical Geology 117, 57-71.

Bédard, J.H., 2005. Partitioning coefficients between olivine and silicate melts. Lithos 83, 394-419.

Bedini, R.M., Bodinier, J.-L., 1999. Distribution of incompatible trace elements between the constituents of spinel peridotite xenoliths: ICP-MS data from the East African Rift. Geochimica et Cosmochimica Acta 63, 3883-3900.

Bell, D., Rossman, G.R., 1992. Water in Earth's mantle: the role of nominally anhydrous minerals. Science 255, 1391-1397.

Berry, A.J., O'Neill, H.St.C, Hermann, J., Scott, D.R., 2007b. The infrared signature of water associated with trivalent cations in olivine. Earth and Planetary Science Letters 261, 134-142.

Berry, A.J., Hermann, J., O'Neill, H.St.C., Foran, G.J., 2005. Fingerprinting the water site in mantle olivine. Geology 33, 869-872.

Berry, A.J., Walker, A.M., Hermann, J., O'Neill H.St.C., Foran G.J., Gale J., 2007a. Titanium substitution mechanisms in forsterite. Chemical Geology 242, 176-186.

Birle, J.D., Gibbs, G.V., Moore, P.B., Smith, J.V., 1968. Crystal structures of natural olivines. American Mineralogist 53, 807-823.

Bizimis, M., Salters, V.J.M., Bonatti, E., 2000. Trace and REE content of clinopyroxenes from supra-subduction zone peridotites. Implications for melting and enrichment processes in island arcs. Chemical Geology 165, 67-85.

Bockrath, C., Ballhaus, C., Holzheid, A., 2004. Fractionation of the platinum-group elements during mantle melting. Science 305, 1951-1953.

Bodinier, J.-L., Dupuy, C., Dostal, J., Merlet, C., 1987. Distribution of trace transition elements in olivine and pyroxenes from ultramafic xenoliths: Application of microprobe analysis. American Mineralogist 72, 902-913.

Boesenberg, J. S., Ebel, D. S., Hewins, R. H., 2004. An experimental study of phosphoran olivine and its significance in main group pallasites (abstract). 35th Lunar and Planetary Science Conference, March 15-19, 2004, League City, Texas, Abstract No. 1366.

Brey, G.P., Köhler, *T*.P., 1990. Geothermobarometry in four-phase lherzolites II. New thermobarometers and practical assessment of existing thermobarometers. Journal of Petrology 31, 1353-1378.

Burns, R.G., 1970. Site preferences of transition metal ions in silicate crystal structures. Chemical Geology 5, 275-283.

Canil, D., O'Neill, H.St.C., 1996. Distribution of ferric iron in some upper-mantle assemblages. Journal of Petrology 37, 609-635.

Colson, R.O., McKay, G.A., Taylor, L.A., 1988. Temperature and composition dependencies of trace element partitioning: olivine/melt and low-Ca pyroxene/melt. Geochimica et Cosmochimica Acta 52, 539-553.

Colson, R.O., McKay, G.A., Taylor, L.A., 1989. Charge balancing of trivalent trace elements in olivine and low-Ca pyroxene: A test using experimental partitioning data. Geochimica et Cosmochimica Acta 53, 643-648.

Deer, W.A., Howie, R.A., Zussman, J. 1997. Rock forming minerals: Orthosilicates. 2 ed., Geological Society of London, 932 pp.

Dobrzhinetskaya, L.F., Bozhilov, K.N., Green, H.W., 1999. The solubility of $TiO_2$ in olivine: implications for the mantle wedge environment. Chemical Geology 160, 357-370.

Dobrzhinetskaya, L.F., Eide, E.A., Larsen, R.B., Sturt, B.A., Trønnes, R.G., Smith, D.C., Taylor, W.R., Posukhova, T.V., 1995. Microdiamond in high-grade metamorphic rocks of the Western Gneiss region, Norway. Geology 23, 597-600.

Dobrzhinetskaya, L.F., Green, H.W., Wang, S., 1996. Alpe Arami: a peridotite massif from depths of more than 300 kilometers. Science 271, 1841-1845.

Dohmen, R., Chakraborty, S., 2007. Fe-Mg diffusion in olivine II: point defect chemistry, change of diffusion mechanisms and a model for calculation of diffusion coefficients in natural olivine. Physics and Chemistry of Minerals 34, 409-430.

Dyar, M.D., McGuire, A.V., Ziegler, R.D., 1989. Redox equilibria and crystal chemistry of coexisting minerals from spinel lherzolite mantle xenoliths. American Mineralogist 74, 969-980.

Dyar, M.D., Delaney, J.S., Sutton, S.R., and Schaefer, M.W., 1998. $Fe^{3+}$ distribution in oxidized olivine: A synchrotron micro-XANES study. American Mineralogist 83, 1361-1365.

Eggins, S.M., Rudnick, R.L., McDonough, W.F., 1998. The composition of peridotites and their minerals: a laser ablation ICP-MS study. Earth and Planetary Science Letters 154, 53-71.

Evans, T.M., O'Neill, H.St.C., Tuff, J., 2008. The influence of melt composition on the partitioning of REEs, Y, Sc, Zr and Al between forsterite and melt in the system CMAS, Geochimica et Cosmochimica Acta 72, 5708-5721.

Finnerty, A.A., Boyd, F. R., 1978. Pressure-dependent solubility of Ca in forsterite coexisting with diopside and enstatite. Carnegie Institution of Washington Yearbook 77, 713-717.

Garrido, C.J., Bodinier, J.-L., Alard, O., 2000. Incompatible trace element partitioning and residence in anhydrous spinel peridotites and websterites from the Ronda orogenic peridotite. Earth and Planetary Science Letters 181, 341-358.

Griffin, W.L., Fisher, N.I., Friedman, J., Ryan, C.G., O'Reilly, S.Y., 1999. Cr-pyrope garnets in the lithospheric mantle. I. Compositional systematics and relations to tectonic setting. Journal of Petrology 40, 679-704.

Griffin, W.L., O'Reilly. S.Y., Natapov. L.M., Ryan. C.G., 2003. The evolution of lithospheric mantle beneath the Kalahari Craton and its margins. Lithos 71, 215-241.

Guggino, S.N., Hervig, R.L., Bell, D.R., 2007. Fluorine in olivines from plutonic, extrusive, and hypabyssal suites (abstract). American Geophysical Union, Fall Meeting 2007, abstract #V41B-0609.

Hauri, E.H., Gaetani, G., Green, T.H., 2006. Partitioning of water during melting of the Earth's upper mantle at $H_2O$ undersaturated conditions. Earth and Planetary Science Letters 248, 715-734.

Hellebrand, E., Snow, J.E., Dick, H.J.B., Hofmann, A.W., 2001. Coupled major and trace elements as indicators of the extent of melting in mid-ocean-ridge peridotites. Nature 410, 677-681.

Hermann J., O'Neill, H.St.C., Berry, A. J., 2005. Titanium solubility in olivine in the system $TiO_2$–MgO–$SiO_2$: no evidence for an ultra-deep origin of Ti-bearing olivine. Contributions to Mineralogy and Petrology 148, 746-760.

Hervig, R.L., Smith, J.V., 1982. Temperature-dependent distribution of Cr between olivine and pyroxene in lherzolite xenoliths. Contributions to Mineralogy and Petrology 81, 184-189.

Hervig, R.L., Smith, J.V., Dawson, J.B., 1986. Lherzolite xenoliths in kimberlites and basalts: Petrogenetic and crystallochemical significance of some minor and trace elements in olivine, pyroxenes, garnet and spinel. Transactions of the Royal Society of Edinburgh: Earth Science 77, pp. 181-201.

Hervig, R.L., Smith, J.V., Steele I.M., 1980b. Fertile and barren Al-Cr-spinel harzburgites from the upper mantle: ion and electron probe analyses of trace elements in olivine and orthopyroxene: relation to lherzolites. Earth and Planetary Science Letters 50, 41-58.

Hervig, R.L., Smith, J.V., Steele I.M., Gurney J.J., Meyer H.O.A., Harris J., 1980a. Diamonds: minor elements in silicate inclusions: pressure-temperature implications. Journal of Geophysical Research 85 (B12), 6919-6929.

Janák, M., Froitzheim, N., Vrabec, M., Krogh Ravna, E.J.K., De Hoog, J.C.M., 2006. Ultrahigh-pressure metamorphism and exhumation of garnet peridotite in Pohorje, Eastern Alps. Journal of Metamorphic Geology 24, 19-31.

Jarosewich, E., Nelen, J.A., Norberg, J.A., 1980. Reference samples for electron microprobe analysis. Geostandards and Geoanalytical Research 4, 43-47.

Jochum, K.P., Nohl, U., 2008. Reference materials in geochemistry and environmental research and the new GeoReM database. Chemical Geology 253, 50-53.

Jurewicz, A.J.G., Watson, B.E., 1988a. Cations in olivine, Part 1. Calcium partitioning and calcium-magnesium distribution between olivines and coexisting melts, with petrological applications. Contributions to Mineralogy and Petrology 99, 176-185.

Jurewicz, A.J.G., Watson, B.E., 1988b. Cations in olivine, Part 2. Diffusion in olivine xenocrysts, with applications to petrology and mineral physics. Contributions to Mineralogy and Petrology 99, 186-201.

Kennedy, C., Kennedy, G., 1976. The equilibrium boundary between graphite and diamond, Journal of Geophysical Reseach 81, 2467-2470.

Kent, A.J.R., Rossman, G.R., 2002. Hydrogen, lithium and boron in mantle-derived olivine: The role of coupled substitutions. American Mineralogist 87, 1432-1436.

Kitamura, M., Kondoh, S., Morimoto, N., Miller, G.H., Rossman, G.R., Putnis, A., 1987. Planar OH-bearing defects in mantle olivine. Nature 328, 143-145.

Klemme, S., 2004. The influence of Cr on the garnet–spinel transition in the Earth's mantle: experiments in the system $MgO–Cr_2O_3–SiO_2$ and thermodynamic modelling. Lithos 77, 639-646.

Köhler, T.P., Brey, G.P., 1990. Calcium exchange between olivine and clinopyroxene calibrated as a geothermobarometer for natural peridotites from 2 to 60 kb with applications. Geochimica et Cosmochimica Acta 54, 2375-2388.

Kohlstedt, D.L., Keppler, H., Rubie, D.C., 1996. Solubility of water in the α, β, and γ phases of $(Mg,Fe)_2SiO_4$. Contributions to Mineralogy and Petrology: 123: 345-357.

Kurosawa, M., Yurimoto, H., Sueno, S., 1997. Patterns in the hydrogen and trace element compositions of mantle olivines. Physics and Chemistry of Minerals 24: 385-395.

Lee, C.-T.A., Harbert, A., Leeman, W.P., 2007. Extension of lattice strain theory to mineral/ mineral rare-earth element partitioning: An approach for assessing disequilibrium and developing internally consistent partition coefficients between olivine, orthopyroxene, clinopyroxene and basaltic melt. Geochimica et Cosmochimica Acta 71, 481-496.

Li, J.-P., O'Neil, H.St.C., Seifert, F., 1995. Subsolidus phase relations in the system MgO-$SiO_2$-Cr-O in equilibrium with metallic Cr, and their significance for the petrochemistry of chromium. Journal of Petrology 36, 107-132.

Lumpkin, G.R., Ribbe, P.H., Lumpkin, N.E., 1983. Composition, order-disorder and lattice parameters of olivines: determinative methods for Mg-Mn and Mg-Ca silicate olivines. American Mineralogist 68, 1174-1182.

Mallmann, G., O'Neill, H.St.C., Klemme, S. 2009. Heterogeneous distribution of phosphorus in olivine from otherwise well-equilibrated spinel peridotite xenoliths and its implications for the mantle geochemistry of lithium. Contributions to Mineralogy and Petrology 158, 485-504.

Matsyuk, S.S., Langer, K., 2004. Hydroxyl in olivines from mantle xenoliths in kimberlites of the Siberian platform. Contributions to Mineralogy and Petrology 147, 413-437.

McDonough, W.F., Stosch, H.-G., Ware, N.G., 1992. Distribution of titanium and the rare earth elements between peridotitic minerals. Contributions to Mineralogy and Petrology 110, 321-328.

McDonough, W.F., Sun, S.-s., 1995. The composition of the Earth. Chemical Geology 120, 223-253.

Mercier, J.-C., Benoit, V. Girardeau, J., 1984. Equilibrium state of diopside-bearing harzburgites from ophiolites: geobarometric and geodynamic implications. Contributions to Mineralogy and Petrology 85, 391-403.

Miller, G.H., Rossman, G.R., Harlow, G.E., 1987. The natural occurrence of hydroxide in olivine. Physics and Chemistry of Minerals 14, 461-472.

Milman-Barris, M.S., Beckett, J.R., Baker, M.B., Hofmann, A.E., Morgan, Z., Crowley, M.R., Vielzeuf, D., Stolper, E., 2008. Zoning of phosphorus in igneous olivine. Contributions to Mineralogy and Petrology 155, 739-765.

Niu, Y., 1997. Mantle melting and melt extraction processes beneath ocean ridges: evidence from abyssal peridotites. Journal of Petrology 38, 1047-1074.

Niu, Y., 2004. Bulk-rock major and trace element compositions of abyssal peridotites: implications for mantle melting, melt extraction and post-melting processes beneath mid-ocean ridges. Journal of Petrology 45, 2423-2458.

O'Reilly, S.Y., Chen, D., Griffin, W.L., Ryan C.G., 1997. Minor elements in olivine from spinel lherzolite xenoliths: implications for thermobarometry. Mineralogical Magazine 61, 257-269.

Ottolini, L., 2002. Accurate SIMS analysis of Ca in olivine based on high-energy doubly charged secondary ions. Journal of Analytical and Atomic Spectrometry 17, 280-283.

Palme, H., O'Neill, H.St.C., 2007. Cosmochemical estimates of mantle composition. Treatise on Geochemistry, Vol. 2.01, pp. 1-38.

Papike, J.J., Karner, J.M., Shearer, C.K., 2005. Comparative planetary mineralogy: Valence-state partitioning of Cr, Fe, Ti and V among crystallographic sites in olivine, pyroxene, and spinel from planetary basalts. American Mineralogist 90, 277-290.

Pearce, N.J.G., Perkins, W.T., Westgate, J.A., Gorton, M.P., Jackson, S.E., Neal, C.R., Chenery, S.P., 1997. A compilation of new and published major and trace element data for NIST SRM 610 and NIST SRM 612 glass reference materials. Geostandards Newsletter 21, 115-144.

Pollack, H.N., Chapman, D.S., 1977. On the regional variation of heat flow, geotherms, and lithospheric thickness. Tectonophysics 38, 279-296.

Pyke, D.R., Naldrett, A.J., Ecktrand, O.R., 1973. Archean ultramafic flows in Munro Township, Ontario. Geological Society of America Bulletin 84, 955-978.

Richmond, N.C., Brodholdt, J.P., 2000. Incorporation of $Fe^{3+}$ into forsterite and wadsleyite. American Mineralogist 85, 1155-1158.

Risold, A.C., Trommsdorff, V., Grobéty, B., 2001. Genesis of ilmenite rods and palisades along humite-type defects in olivine from Alpe Arami. Contributions to Mineralogy and Petrology 140, 619-628.

Rohrbach, A., Ballhaus, C., Golla-Schindler, U., Ulmer, P., Kamenetsky, V.S., Kuzmin, D.V., 2007. Metal saturation in the upper mantle. Nature 449, 456-458.

Seitz, H.-M., Woodland, A.B., 2000. The distribution of lithium in peridotitic and pyroxenitic mantle lithologies - an indicator of magmatic and metasomatic processes. Chemical Geology 166, 47-64.

Shannon, R.D., 1976. Revised effective ionic radii and systematic studies of interatomic distances in halides and chalcogenides. Acta Crystallographica A32, 751-767.

Simon, N.S.C., Carlson, R.W., Pearson, G.D., Davies, G.R., 2007. The origin and evolution of the Kaapvaal cratonic lithospheric mantle. Journal of Petrology 48, 589-625.

Smit, Y., Schiano,, Faure, F., De Hoog, J.C.M., Stuart, F., 2005. Melt inclusions in olivine phenocrysts (Fo 91-93) from Tertiary picrites from Padloping Island, Baffin Island: the earliest melts generated by the Iceland Plume? (abstract). EGU 2005, Vienna, Geophysical Research Abstracts 7, Abstract 11069.

Sobolev, N.V., Logvinova, A.M., Zedgenizov, D.A., Pokhilenko, N.P., Kuzmin, D.V., Sobolev, A., 2008. Olivine inclusions in Siberian diamonds: high-precision approach to minor elements. European Journal of Mineralogy 20, 305-315.

Spandler, C., O'Neill, H. St C., Kamenetsky, V. S., 2007. Survival times of anomalous melt inclusions from element diffusion in olivine and chromite. Nature 447, 303-306.

Spengler, D., 2006. Origin and evolution of deep upper mantle rocks from western Norway (Ph.D. Thesis). Geologica Ultraiectina 266, Utrecht University, The Netherlands, 266p.

Stachel, T., Aulbach, S., Brey, G.P., Harris, J.W., Leost, I., Tappert, R., Viljoen, K.S., 2004. The trace element composition of silicate inclusions in diamonds: a review. Lithos 77, 1-19.

Stosch, H-G., 1981. Sc, Cr, Co and Ni partitioning between minerals from spinel peridotite xenoliths. Contributions to Mineralogy and Petrology 78, 166-174.

Taura, H., Yurimoto, H., Kurita, K., Sueno., 1998. Pressure dependence on partition coefficients for trace elements between olivine and coexisting melts. Physics and Chemistry of Minerals 25, 469-484.

Tinker, D., Lesher, C.E., 2001. Solubility of $TiO_2$ in olivine from 1 to 8 GPa. Eos Transactions AGU 82, Fall Meeting Supplement, Abstract V51B-1001.

Ulmer, P., Risold, A.C., Trommsdorff, V., 1998. $TiO_2$ solubility in mantle olivine as a function of pressure, temperature, a($SiO_2$), and f($H_2$). Eos Transactions AGU 79, Fall Meeting Supplement, Abstract V12A-06.

Wan, Z., Coogan, L.A., Canil, D., 2008. Experimental calibration of aluminum partitioning between olivine and spinel as a geothermometer. American Mineralogist 93, 1142-1147.

Webb, K.J., Scott Smith, B.H., Paul, J.L., Hetman, C.M., 2004. Geology of the Victor Kimberlite, Attawapiskat, Northern Ontario, Canada: cross-cutting and nested craters. Lithos 76, Selected Papers from the Eighth International Kimberlite Conference, Volume 1, pp. 29-50.

Witt-Eickschen G., O'Neill, H.St.C., 2005. The effect of temperature on the equilibrium distribution of trace elements between clinopyroxene, orthopyroxene, olivine and spinel in upper mantle peridotite. Chemical Geology 221, 65-101.

Wood, B.J., Blundy, J.D., 2003. Trace element partitioning under crustal and uppermost mantle conditions: the influence of ionic radius, cation charge, pressure, and temperature. In: Holland, H.D., Turekian., K.K. (Eds.-in-Chief), The mantle and core. Treatise on Geochemistry, Volume 2, pp. 425-449.

Zangana, N.A., Downes, H., Thirlwall, M.F., Hegner, E., 1997. Relationship between deformation, equilibration temperatures, REE and radiogenic isotopes in mantle xenoliths (Ray Pic, Massif Central, France): an example of plume-lithosphere interaction? Contributions to Mineralogy and Petrology 127, 187-203.

## Tables

### Table 1. Sample locations

| location | source rock | lithologies [a] | latitude | longitude |
|---|---|---|---|---|
| Kaalvallei, South-Africa | kimberlite pipe | gt±sp lhz | 28° 02' S | 26° 50' E |
| Kimberley, South-Africa | kimberlite pipe | gt±sp lhz, hrz | 28° 44' S | 24° 47' E |
| Premier, South-Africa | kimberlite pipe | gt±sp lhz, hrz | 25° 40' S | 28° 31' E |
| Kirkland Lake, Canada | kimberlite pipe | gt±sp lhz, hrz | 48° 16' N | 79° 52' W |
| Labait, Tanzania | alkali basalt | gt, sp lhz | 04° 34' S | 35° 26' E |
| Ray Pic, France | alkali basalt | sp lhz | 44° 50' N | 04° 20' E |
| Otroy, Norway | orogenic | gt±sp lhz, hrz | 62° 42' N | 06° 42' E |
| Pohorje, Slovenia | orogenic | gt-sp lhz | 46° 24' N | 15° 29' E |
| Ronda, Spain | orogenic | sp lhz | 36° 30' N | 05° 11' W |

[a] gt = garnet, sp = spinel, lhz = lherzolite, hrz = harzburgite (clinopyroxene absent)

**Table 2. SEM-EDS data obtained from mineral standards**

| Mineral | Olivine | | Diopside | | Omphacite | | Hypersthene | | Garnet | |
|---|---|---|---|---|---|---|---|---|---|---|
| Location | San Carlos, AZ | | Natural Bridge, NY | | Roberts Victor Mine | | Johnstown meteorite | | Roberts Victor Mine | |
| USNM# | 111312/44 | | 117733 | | 110607 | | 746 | | 110752 | |
| | (n=4) | cert. | (n=3) | cert. | (n=3) | cert. | (n=3) | cert. | (n=3) | cert. |
| $SiO_2$ | 40.34 (9) | 40.69 | 55.59 (5) | 55.15 | 56.04(10) | 55.58 | 54.28 (9) | 53.96 | 39.92 (3) | 40.16 |
| $TiO_2$ | | | | | 0.38 (1) | 0.37 | 0.12 (3) | 0.16 | 0.38 (2) | 0.35 |
| $Al_2O_3$ | | | 0.13 (2) | 0.11 | 8.83 (1) | 8.91 | 1.10 (2) | 1.23 | 22.52 (5) | 22.70 |
| $Cr_2O_3$ | | | | | | | 0.74 (1) | 0.75 | | |
| FeO | 9.67 (5) | 9.52 | 0.24 (3) | 0.24 | 4.32 (5) | 4.63 | 15.14 (4) | 15.18 | 11.45 (7) | 11.31 |
| MnO | 0.13 (2) | 0.14 | | | 0.08 (1) | 0.10 | 0.48 (1) | 0.49 | 0.17 (1) | 0.19 |
| MgO | 49.48 (6) | 49.28 | 18.22 (2) | 18.39 | 11.49 (6) | 11.60 | 26.69 (1) | 26.72 | 7.41 (2) | 7.17 |
| CaO | | | 25.61 (5) | 25.76 | 13.70 (4) | 13.79 | 1.43 (1) | 1.52 | 18.13 (3) | 18.12 |
| $Na_2O$ | | | 0.21 (3) | 0.34 | 5.16 (3) | 5.01 | | | | |
| NiO | 0.38 (1) | 0.37 | | | | | | | | |
| Mg# | 90.12 (7) | 90.22 | 99.3 | 99.3 | 82.6 | 81.7 | 75.9 | 75.8 | 53.6 | 53.1 |

All Fe as FeO. 1σ standard deviations indicated between parentheses represent variation in last digit. Certified values from Jarosewich et al. (1980).

**Table 3. Laser and solution ICP-MS and ion probe data of olivine standards**

| | DC0212 laser ICP-MS Oxford (n=5) | DC0212 ion probe Edinburgh (n=15) | DC0212 solution ICP-MS GVC (n=4) | San Carlos #1 laser ICP-MS Oxford (n=2) | San Carlos #1 laser ICP-MS GVC (n=2) | San Carlos #1 ion probe Edinburgh (n=2) | San Carlos #2 ion probe Edinburgh (n=4) |
|---|---|---|---|---|---|---|---|
| Li | 1.46 (7) | 1.09 (5) | 1.4 (5) | | 1.9 | 1.17 | 1.08 (3) |
| Na | 61 (4) | 62 (4) | 115 (59) | 68 | 82 | 77 | 55 (15) |
| Al | 39 (2) | 39 (3) | 77 (22) | 196 | 174 | 172 | 104 (10) |
| P | 46 (4) | | | 42 | 32 | | |
| Ca | 174 (9) | 150 (2) | 252 (42) | 625 | 665 | 552 | 563 (7) |
| Sc | 0.77 (8) | 0.66 (9) | 1.0 (3) | 3.2 | 2.7 | 2.4 | 3.04 (6) |
| Ti | 14.9 (6) | 12 (1) | 22 (2) | 25 | 24 | 19 | 9.7 (5) |
| V | 4.9 (3) | 4.0 (3) | 5.1 (3) | 4.2 | 4.5 | 4.0 | 2.7 (3) |
| Cr | 181 (10) | 167 (8) | 205 (26) | 103 | 108 | 107 | 146 (2) |
| Mn | 695 (13) | 670 (12) | 724 (23) | 1057 | 1085 | 1098 | 1117 (20) |
| Co | 137 (3) | 157 (9) | 143 (3) | 142 | 143 | 186 | 179 (6) |
| Ni | 3300 (200) | 3450 (50) | | 2950 | 2840 | | |
| Cu | 2.7 (2) | <5 | 6 (1) | 0.9 | 1.7 | | |
| Zn | 54.9 (8) | 46 (5) | | 54 | 58 | | |
| Ga | 0.049 (1) | | | 0.062 | | | |
| As | <0.1 | | | | | | |
| Rb | <0.008 [a] | 0.06 (2) | | | | | |
| Sr | <0.01 [a] | 0.14 (5) | | <0.01 | | | |
| Y | <0.002 | 0.007 (2) | 0.04 (1) | 0.06 | 0.07 | 0.115 | 0.059 (7) |
| Zr | 0.06 (2) | 0.14 (5) | 0.14 (7) | 0.003 | 0.009 | <0.1 | <0.1 |
| Nb | 0.24 (3) | 0.33 (6) | 0.23 (3) | 0.0005 | <0.02 | <0.05 | <0.05 |
| Mo | 0.022 (5) | | | 0.023 | | | |
| In | 0.006 (2) | | | | | | |
| Sn | 0.52 (3) | | | | | | |
| Sb | 0.022 (2) | | | | | | |
| Ba | <0.006 [a] | 0.28 (6) | | | <0.005 | | |
| Ce | <0.003 [a] | 0.16 (4) | | | <0.002 | | |
| Pb | 0.038 (5) [a] | 1.2 (3) | | | | | |
| Th | 0.006 (2) [a] | 0.03 (1) | | | | | |
| U | 0.0002 (1) [a] | 0.14 (5) | | | | | |

DC0212 is an in-house olivine standard prepared from a garnet peridotite from the Kimberley kimberlite pool. Values in the first column were used for calibration of olivine data presented in this study. San Carlos #1 olivine is same grain as in Table 2, whereas San Carlos #2 is a grain from a different lab (Edinburgh). Values between parentheses are 1s uncertainties in the last digit of the average. [a] Data collected at GVC.

## Table 4. Selected olivine major and trace element compositions

| sample | 54-24 | B-P1 | FB1301 | DC0212 | 54-102 | A1-P6 | C-P7 | DC0336 | 54-8 | DC0322 | RP91-10 | RP83-71 | RP91-2 | DS0278 | 119-5 | RoP01 | BI-6 | DB01-7 |
|---|---|---|---|---|---|---|---|---|---|---|---|---|---|---|---|---|---|---|
| *lithology* | *gt lhz* | *gt lhz* | *gt lhz* | *gt lhz* | *gt lhz* | *gt lhz* | *gt lhz* | *gt hrz* | *gt-sp lhz* | *sp hrz* | *sp lhz* | *sp lhz* | *sp lhz* | *gt lhz* | *gt-sp lhz* | *sp lhz* | *picrite* | *kimberl* |
| *origin* | *xeno* | *xeno* | *xeno* | *xeno* | *xeno* | *xeno* | *xeno* | *xeno* | *xeno* | *xeno* | *xeno* | *xeno* | *xeno* | *orog* | *orog* | *orog* | *volc* | *volc* |
| *locality* | *KV* | *KL* | *Premier* | *Kimb* | *KV* | *KL* | *KL* | *Kimb* | *KV* | *Kimb* | *Ray Pic* | *Ray Pic* | *Ray Pic* | *Norway* | *Pohorje* | *Ronda* | *Baffin Isl* | *Canada* |
| $SiO_2$ wt.% | 40.40 | 40.41 | 40.24 | 40.47 | 40.49 | 40.53 | 41.18 | 40.69 | 40.97 | 40.38 | 41.10 | 41.43 | 41.22 | 40.65 | 40.00 | 40.17 | 40.27 | 40.70 |
| FeO | 8.55 | 9.28 | 9.40 | 7.73 | 7.51 | 7.99 | 8.04 | 6.70 | 6.76 | 8.31 | 9.33 | 8.97 | 9.55 | 7.30 | 10.51 | 8.91 | 7.74 | 7.52 |
| MnO | 0.10 | 0.12 | 0.12 | 0.07 | 0.09 | 0.07 | 0.12 | 0.06 | 0.08 | 0.11 | 0.13 | 0.12 | 0.13 | 0.06 | 0.10 | 0.16 | 0.11 | 0.12 |
| MgO | 50.41 | 49.58 | 49.62 | 51.18 | 51.41 | 50.97 | 50.21 | 52.02 | 51.72 | 50.75 | 48.95 | 49.03 | 48.72 | 51.61 | 49.05 | 50.17 | 50.82 | 51.33 |
| NiO | 0.39 | 0.33 | 0.37 | 0.46 | 0.42 | 0.36 | 0.35 | 0.44 | 0.41 | 0.37 | 0.32 | 0.36 | 0.29 | 0.33 | 0.31 | 0.51 | 0.44 | *0.25* |
| #Si (4 oxygens) | 0.987 | 0.990 | 0.987 | 0.986 | 0.985 | 0.988 | 1.002 | 0.986 | 0.992 | 0.986 | 1.005 | 1.011 | 1.008 | 0.987 | 0.986 | 0.984 | 0.982 | 0.989 |
| #Mg | 1.837 | 1.811 | 1.815 | 1.858 | 1.865 | 1.851 | 1.821 | 1.880 | 1.867 | 1.847 | 1.785 | 1.783 | 1.777 | 1.868 | 1.802 | 1.833 | 1.848 | 1.860 |
| #$Fe^{2+}$ | 0.175 | 0.190 | 0.193 | 0.158 | 0.153 | 0.163 | 0.164 | 0.136 | 0.137 | 0.170 | 0.191 | 0.183 | 0.195 | 0.148 | 0.217 | 0.183 | 0.158 | 0.153 |
| #Mn | 0.002 | 0.003 | 0.003 | 0.001 | 0.002 | 0.001 | 0.002 | 0.001 | 0.002 | 0.002 | 0.003 | 0.003 | 0.003 | 0.001 | 0.002 | 0.003 | 0.002 | 0.002 |
| #Ni | 0.008 | 0.007 | 0.007 | 0.009 | 0.008 | 0.007 | 0.007 | 0.009 | 0.008 | 0.007 | 0.006 | 0.007 | 0.006 | 0.006 | 0.006 | 0.010 | 0.009 | 0.006 |
| Total | 3.008 | 3.001 | 3.005 | 3.012 | 3.013 | 3.010 | 2.995 | 3.011 | 3.006 | 3.012 | 2.990 | 2.987 | 2.989 | 3.012 | 3.013 | 3.013 | 2.998 | 3.011 |
| Fo | 91.3% | 90.5% | 90.4% | 92.2% | 92.4% | 91.9% | 91.8% | 93.3% | 93.2% | 91.6% | 90.3% | 90.7% | 90.1% | 92.6% | 89.3% | 90.9% | 92.1% | 92.4% |
| Li ppm | 2.26 | 1.89 | 1.91 | 1.46 | 1.33 | 1.50 | 1.21 | 0.99 | 1.29 | 1.44 | 2.0 | 2.1 | 1.38 | 1.02 | 2.32 | 0.96 | 0.94 | 2.87 |
| Na | 304 | 476 | 506 | 61 | 85 | 90 | 94 | 122 | 28 | 26 | 126 | 46 | 48 | 7.6 | 2.0 | 13.7 | 109 | 27.2 |
| Al | 94 | 214 | 210 | 39 | 24 | 18 | 27 | 46 | 9.0 | 0.58 | 160 | 48 | 43 | 5.5 | 2.0 | 25 | 840 | 1.00 |
| P | 39.1 | 36 | 35.0 | 46.2 | 26.7 | 31 | 40 | 60.2 | 4.9 | 25.8 | 35 | 31 | 31 | 19 | 26 | 24 | 40 | 61 |
| Ca | 186 | 575 | 472 | 174 | 92 | 69 | 74 | 128 | 54 | 27 | 524 | 207 | 211 | 56 | 24 | 215 | 2379 | 55.0 |
| Sc | 1.29 | 1.83 | 1.49 | 0.77 | 0.44 | 0.66 | 0.62 | 0.66 | 0.64 | 1.37 | 2.7 | 1.82 | 2.0 | 0.4 | 0.38 | 1.89 | 5.3 | 0.77 |
| Ti | 132 | 167 | 81 | 14.9 | 10.6 | 109 | 175 | 4.2 | 0.58 | 107 | 24.4 | 9.0 | 11.3 | 1.36 | 13.3 | 3.2 | 52 | 63.1 |
| V | 6.3 | 10.4 | 9.40 | 4.94 | 2.19 | 2.9 | 3.8 | 4.16 | 1.57 | 1.84 | 3.0 | 1.35 | 1.22 | 1.29 | 0.067 | 1.05 | 6.4 | 1.12 |
| Cr | 183 | 604 | 249 | 181 | 87 | 104 | 83 | 147 | 47 | 41 | 120 | 28.3 | 42 | 25.4 | 1.45 | 48 | 1390 | 26.5 |
| Mn | 488 | 851 | 803 | 695 | 499 | 707 | 619 | 541 | 509 | 800 | 974 | 923 | 998 | 555 | 658 | 915 | 879 | 957 |
| Co | 87 | 126 | 130 | 137 | 113 | 132 | 127 | 124 | 122 | 120 | 128 | 126 | 124 | 129 | 143 | 125 | 122 | 112 |
| Ni | 2041 | 2506 | 2730 | 3307 | 2832 | 2890 | 2897 | 3260 | 3100 | 2751 | 2660 | 2812 | 2667 | 2754 | 1737 | 2679 | 3217 | 1846 |
| Cu | 2.0 | 3.3 | 3.3 | 2.7 | 1.3 | 1.6 | 1.6 | 1.5 | 1.3 | 1.1 | 1.9 | 1.4 | 1.2 | 1.1 | 1.1 | 1.0 | 3.5 | 0.75 |
| Zn | 37.2 | 63 | 62.6 | 54.9 | 44.1 | 59 | 54 | 44.9 | 27.8 | 52.6 | 52.8 | 40.2 | 40.6 | 47 | 60 | 37.7 | 57 | 43.8 |
| Y | <0.002 | 0.017 | 0.018 | <0.002 | <0.002 | <0.002 | <0.002 | <0.002 | <0.002 | <0.002 | 0.060 | 0.018 | 0.019 | <0.002 | <0.002 | <0.002 | 0.148 | 0.014 |
| Zr | 0.171 | 0.12 | 0.035 | 0.066 | 0.055 | 0.07 | 0.21 | 0.26 | 0.012 | 0.04 | 0.025 | <0.005 | 0.011 | <0.005 | 0.006 | 0.005 | <0.005 | 0.09 |
| Nb | na | 0.016 | 0.025 | 0.238 | na | 0.03 | 0.26 | 0.57 | na | 0.14 | <0.01 | <0.01 | <0.01 | na | na | na | <0.01 | 4.68 |
| Cr# ol | 0.50 | 0.59 | 0.38 | 0.71 | 0.65 | 0.75 | 0.61 | 0.63 | 0.73 | 0.97 | 0.28 | 0.23 | 0.33 | 0.71 | 0.27 | 0.50 | 0.44 | 0.93 |
| *P* (2Px, kb) | 61.0 | 60.4 | 67.5 | 43.8 | 40.9 | 39.2 | 41.8 | - | 31.0 | - | 15.0 | 15.0 | 15.0 | 29.3 | 32.0 | 15.0 | - | - |
| *T* (2Px, °C) | 1256 | 1389 | 1404 | 1066 | 967 | 958 | 972 | - | 843 | - | 1055 | 828 | 865 | 776.8 | 775 | 894 | - | - |
| *P* (Ca-Opx) | 58.9 | 69.3 | 74.6 | 45.0 | 41.0 | 33.5 | 41.6 | 42.1 | 31.5 | 20.0 | 15.0 | 15.0 | 15.0 | 26.6 | 32.1 | 15.0 | - | - |
| *T* (Ca-Opx) | 1225 | 1522 | 1507 | 1087 | 970 | 870 | 969 | 1036 | 851 | 810 | 1039 | 914 | 922 | 731 | 777 | 1008 | - | - |
| *P* (Al-Ol, kb) | 60.2 | 64.2 | 68.8 | 43.2 | 41.4 | 38.0 | 43.0 | 43.7 | 30.1 | 20.0 | 15.0 | 15.0 | 15.0 | 30.6 | 21.0 | 15.0 | - | - |
| *T* (Al-Ol, °C) | 1244 | 1447 | 1422 | 1057 | 976 | 940 | 992 | 1066 | 826 | 605 | 1013 | 841 | 848 | 798 | 593 | 819 | - | - |

Major elements in wt.% oxide by SEM-EDS normalised to 100%; trace elements in ppm by LA-ICP-MS. <dl = < detection limit. na = not analysed. Lithology abbreviations: gt = garnet; sp = spinel; lhz = lherzolite; hrz = harzburgite; xeno = xenolith; orog = orogenic; volc = volcanic. Locatilities: KL = Kirkland Lake; KV = Kaalvallei; Kimb = Kimberley. Cr# = atomic Cr/(Cr+Al). Pressure and temperature estimates: 2Px = two pyroxene thermometer (Brey and Kohler, 1990) with Al-in-Opx barometer (Brey and Kohler, 1990); Ca-Opx = Ca-in-Opx thermometer (Brey and Kohler, 1990) with Al-in-Opx barometer (Brey and Kohler, 1990); P (Al-Ol) = P(Al-Ol) with T from T(2Px) or T(Ca-Opx); T(Al-Ol) = T(Al-Ol) with P from P(2Px) or P(Ca-Opx). If no garnet was present in the sample a fixed pressure of 15 or 20 kbar was used for any of the above.

**Table 5. Olivine-mineral partition coefficients**

| | *a1* | *a2* | *a3* | *a4* | *RMSE* |
|---|---|---|---|---|---|
| $\log D_{\mathrm{Al}}^{ol/gt}$ | -4688 | -7.306 | | -0.119 | *0.0059* |
| $\log D_{\mathrm{Al}}^{ol/cpx}$ | -4409 | -6.250 | -2.914 | 1.278 | *0.0052* |
| $\log D_{\mathrm{Cr}}^{ol/gt}$ | -2485 | 1.343 | | -0.615 | *0.0115* |
| $\log D_{\mathrm{Cr}}^{ol/cpx}$ | -3852 | -5.534 | -2.687 | 1.381 | *0.0061* |
| $\log D_{\mathrm{V}}^{ol/cpx}$ | -3755 | -22.340 | -2.435 | 2.029 | *0.0160* |
| $\log D_{\mathrm{Sc}}^{ol/gt}$ | -1833 | 2.233 | | -0.780 | *0.0028* |
| $\log D_{\mathrm{Ca}}^{ol/cpx}$ | -1846 | -10.136 | -1.317 | -0.729 | *0.0058* |
| $\log D_{\mathrm{Na}}^{ol/cpx}$ | -3826 | -7.610 | -2.335 | 1.275 | *0.0197* |
| $\log D_{\mathrm{Ti}}^{ol/cpx}$ | -1040 | -5.633 | -0.519 | -0.201 | *0.0368* |
| $\log D_{\mathrm{Co}}^{ol/cpx}$ | 988 | -3.137 | 0.647 | 0.134 | *0.0028* |

Partition coefficients for Al, Cr, Ca, Na and Ti are based on $N_i^{\mathrm{ol}} / N_i^{\mathrm{min}}$ where $N_i$ is number of atoms of element *i* per formula unit of four (olivine), six (clinopyroxene) or twelve (garnet) oxygens. Those for Sc, Co and V are based on concentrations in ppm in both minerals. Fitted equation: $\log D = a1/T + a2\,P/T + a3\,\#\mathrm{Na}_{\mathrm{cpx}} + a4$. RMSE = root mean square error = √(sum of squared residuals / (n-2))

**Figure Captions**

Fig. 1 Ionic radii and oxidation states of cations that partition into the olivine structure. Ionic radii after Shannon (1976) with all transition metals in high-spin state (Burns, 1970). Cation charges are only indicated for subordinate oxidation states under normal mantle conditions. The optimum size of a site depends on the charge of the cation, and is 0.72 Å for 2+ and 1+ ions in the olivine M1,2 site, 0.71 Å for 3+ ions, and slightly smaller for higher oxidation states (Wood and Blundy, 2003).

Fig. 2 Iteratively calculated equilibrium *P* and *T* conditions of the samples presented in this study. Closed symbols are calculated using the 2px thermometer (Brey and Kohler, 1990), whereas open symbols were calculated by Ca-in-Opx thermometry (Brey and Kohler, 1990). Pressures of garnet-bearing samples are calculated from Al-in-Opx barometry (Brey and Kohler, 1990), whereas the pressure was set at 15 or 20 kbar for remaining samples. Conductive geothermal gradients (surface heat flow in $mW/m^2$) are from Pollack and Chapman (1977). The diamond graphite transition is from Kennedy and Kennedy (1976). Also indicated is the garnet-spinel transition for $Cr_2O_3$-free lithologies (gt in); the presence of $Cr_2O_3$ enhances the stability field of spinel to higher pressures (Klemme, 2004). Sample suites: KV = Kaalvallei kimberlite pipe, South-Africa; KL = Kirkland Lake kimberlite cluster, Ontario, Canada; Kimb = Kimberley kimberlite pool, South-Africa; FB = Premier kimberlite pipe, South-Africa; AT = Labait volcano, Tanzania; Ray Pic = Ray Pic volcano, France. Other localities are orogenic peridotites from Ronda (Spain), Otroy (Norway) and Pohorje (Slovenia).

Fig. 3 Concentrations of Group I elements in olivine vs. forsterite contents for various mantle lithologies. Compositional fields are for kimberlitic olivine (*k*) from Victor

Pipe, Canada; (dotted line) and picritic lavas (*v*) from Baffin Island, Canada (continuous line). Dashed horizontal line indicates primitive mantle values after McDonough and Sun (1995) and Palme and O'Neill (2007).

Fig. 4 Concentrations of Group II elements against equilibration temperature of the samples in log C vs. 1000/*T*(K) for various mantle lithologies. Compositional ranges of kimberlitic (*k*) and volcanic olivine (*v*) at approximate magmatic temperatures of 1400 and 1250°C are indicated by dark and light grey bars, respectively. Compositions of co-existing minerals (garnet, gt: circles; clinopyroxene, cp: inverted triangles; orthopyroxene, op: tilted triangles) are indicated for comparison.

Fig. 5 Concentrations of Group III elements against equilibration temperature of the samples for different mantle lithologies in log C vs. 1000/*T*(K). Compositional ranges of kimberlitic and picritic olivine as in Figure 4. Samples below detection limit were plotted at the detection limit value (indicated by DL). Crosses represent solution ICP-MS data of spinel peridotites from Witt-Eickschen and O'Neill (2005).

Fig. 6 Co-variation of Co, Al and Ti in olivine with clinopyroxene (A) and garnet (B). Dashed lines indicate constant $D^{ol/min}$ values. Group 1 elements, such as Co, are nearly constant in olivine, but variable in cpx and grt. Group 2 elements, such as Al, are nearly constant in garnet and cpx but vary considerably in olivine, whereas Group 3 elements such as Ti are variable in both, with nearly constant D values.

Fig. 7 Discrimination diagrams to identify various mantle lithologies based on olivine composition. (A) Log Zr vs. Sc diagram showing nearly perfect separation between different mantle lithologies. Plus symbols represent solution ICP-MS data for spinel peridotites from Witt-Eickschen and O'Neill (2005). (B) Mn versus log Al diagram showing reasonable separation between different mantle lithologies using elements

that can be measured by electron microprobe. Most of the mismatched samples (dashed symbols) are harzburgites.

Fig. 8 Diagram of whole-rock $TiO_2$ contents vs. $TiO_2$ contents of constituent minerals for garnet-bearing peridotites from Kaalvallei (large symbols) and spinel peridodites from Ray Pic (small symbols). Kaalvallei whole-rock values are reconstructed from modal mineral abundances and compositions (Electronic Appendix 1), whereas those from Ray Pic are from Zangana et al. (1999). Also indicated are whole-rock values for the primitive mantle (PM; McDonough and Sun, 1995), the range of abyssal peridotites (Niu, 2004) and supra-subduction zone peridotites (SSZ; after Bizimis et al., 2000). Note that the relation between whole rock and olivine Ti content is very similar in garnet and spinel peridotites.

Fig. 9 Variation of olivine Cr# (molar Cr/(Cr+#Al)) with Cr# of co-existing mantle minerals. Excellent correlations are observed for olivine (OL), clinopyroxene (CPX), orthopyroxene (OPX) and spinel (SP), but less good for garnet (GT).

Fig. 10 (A) Diagram of Cr and Al in olivine (atoms p.f.u.) showing the variation in olivine Cr# of the samples. Olivine from most garnet peridotites are characterised by high Cr# of 0.5-0.75, whereas olivine from most spinel peridotites has Cr# less than 0.4. (B) Plot of Na vs. Al and Cr in olivine (atoms p.f.u.). Garnet-bearing peridotites are indicated by black symbols, whereas open symbols indicate spinel peridotites from the same sample suite. Spinel peridotites (Ray Pic) show excess Al+Cr compared to garnet peridotites, which can be fully attributed to excess Al (see text). See Fig. 2 for abbreviations of sample suites.

Fig. 11 Olivine-mineral partition coefficients for various elements plotted against temperature for samples from the Kaalvallei suite.

Fig. 12 (A) Co-variation of Al with *T* in a 1000/*T*(K) vs. ln Al (ppm) diagram. Dashed and continuous lines represent calculated Al contents for given temperature based on the Al-ol thermobarometer (Eq. 12) for various pressures at olivine Cr# 0.45 and 0.15, respectively. Small numbers next to lines indicate *P* and olivine Cr#. For abbreviations of sample suites see Fig. 2. (B) Comparison of temperatures (°C) calculated from two-pyroxene thermometer (Brey and Kohler, 1990) and Al-ol(Cr#) thermometer, respectively, using an iterative calculation with Al-in-opx barometry (Brey and Kohler, 1990), except for harzburgites, for which the Ca-in-opx thermometer was used (Brey and Kohler, 1990). Dashed lines indicate 50°C temperature intervals. Even though only garnet lherzolites were used in the calibration of the Al-ol(Cr#) thermometer, the temperature estimates for other lithologies are excellent and show its wide applicability. Only mosaic-textured peridotites (open diamonds) consistently give anomalous temperatures and were therefore excluded from the calibration.

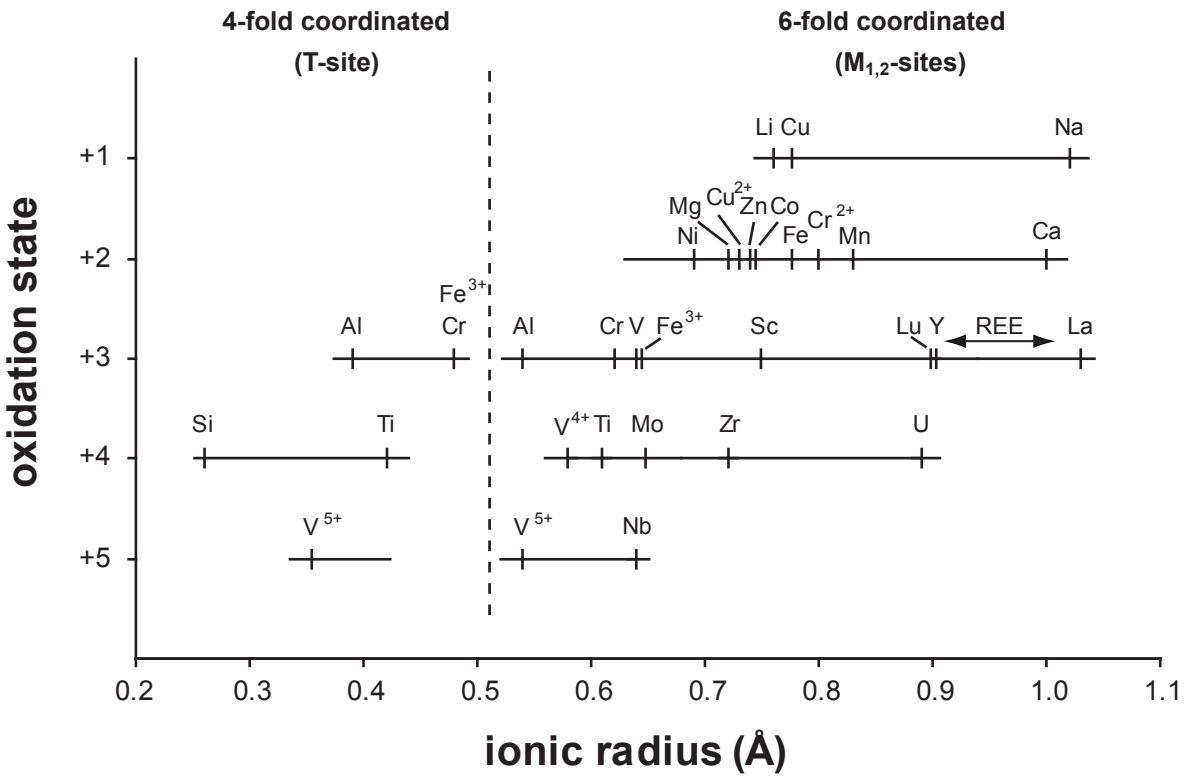


Fig. 1. De Hoog (submitted to Chem Geol)

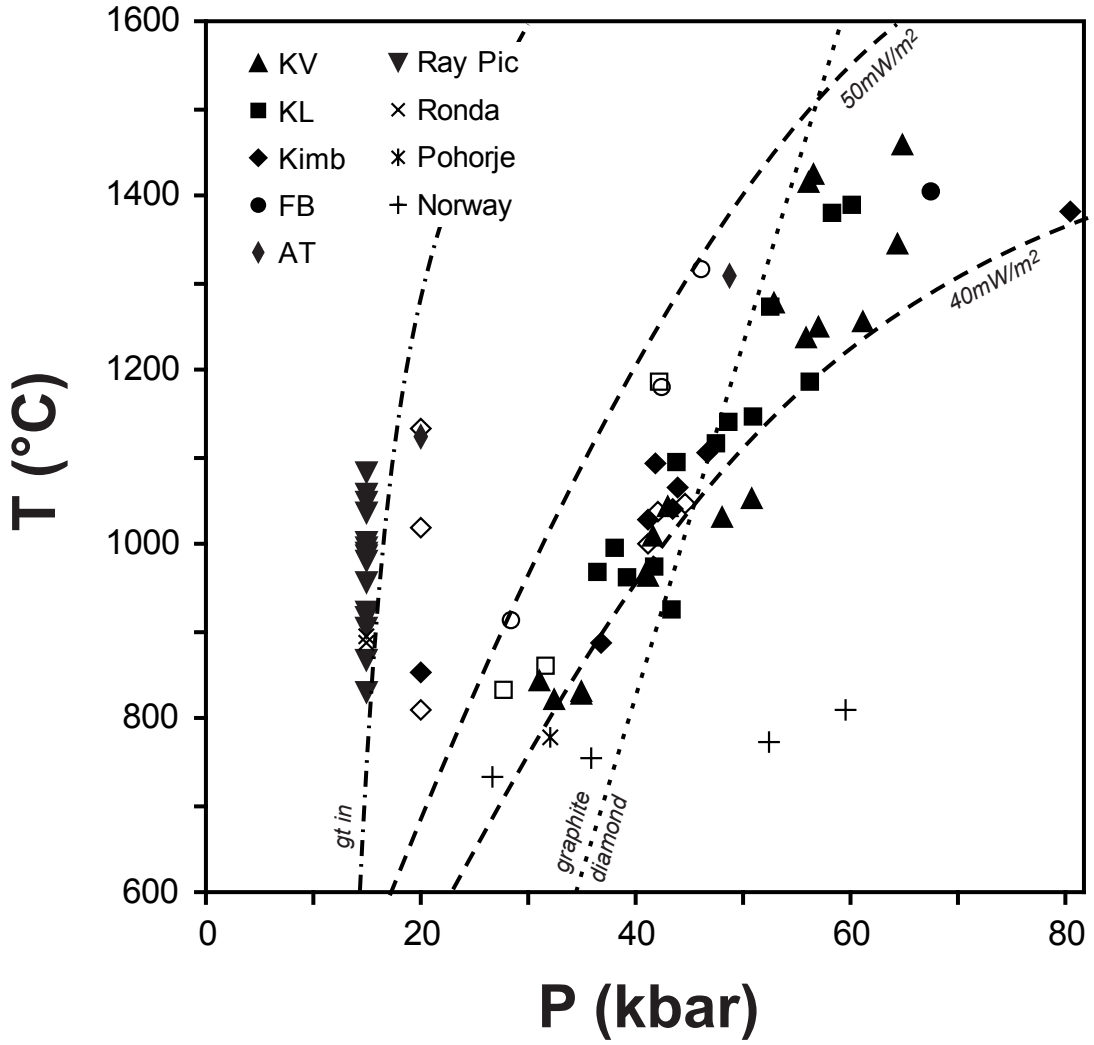


Fig. 2. De Hoog (submitted to Chem Geol)

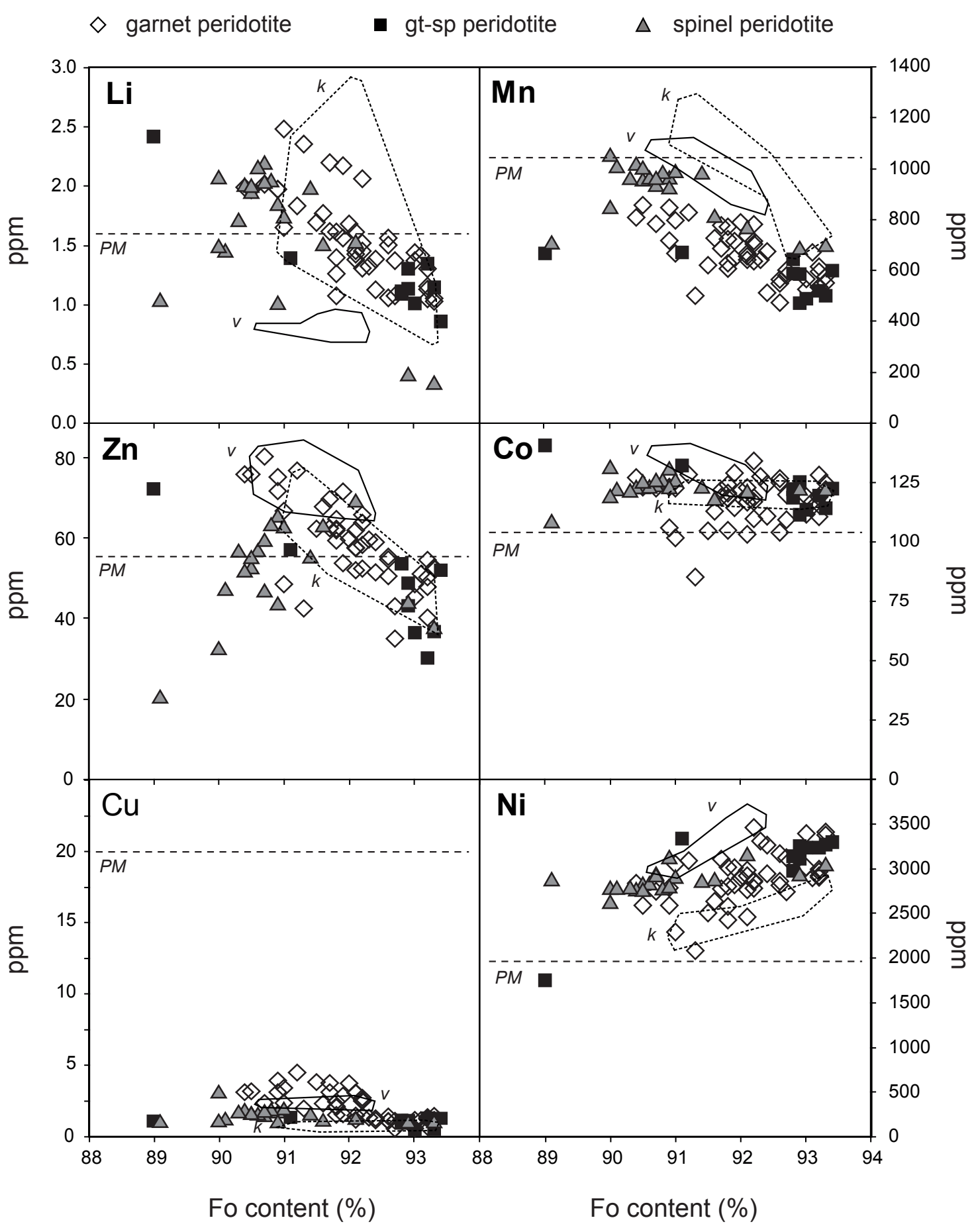


Fig 3. De Hoog (submitted to ChemGeol)

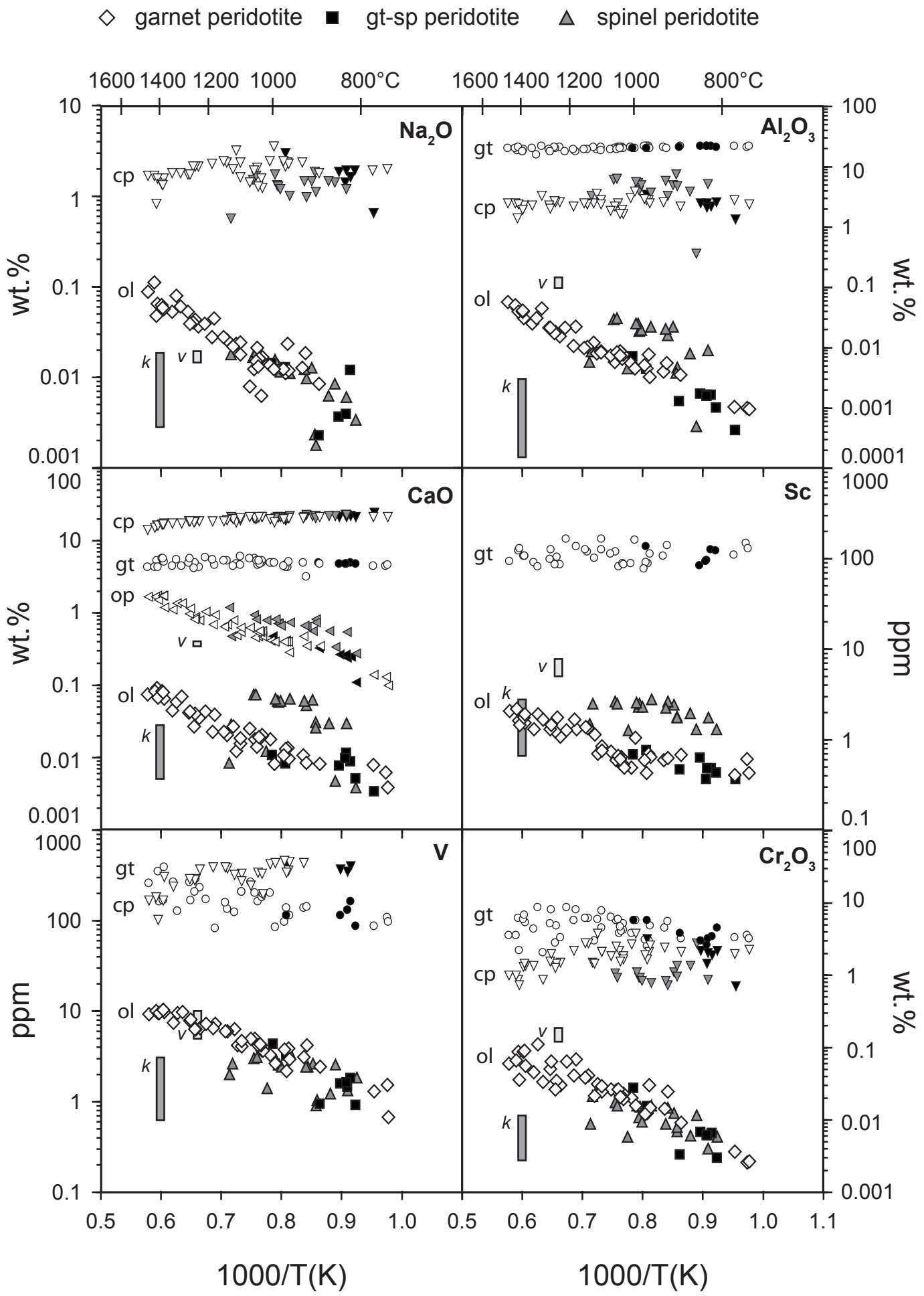


Fig. 4 De Hoog (submitted to Chem Geol)

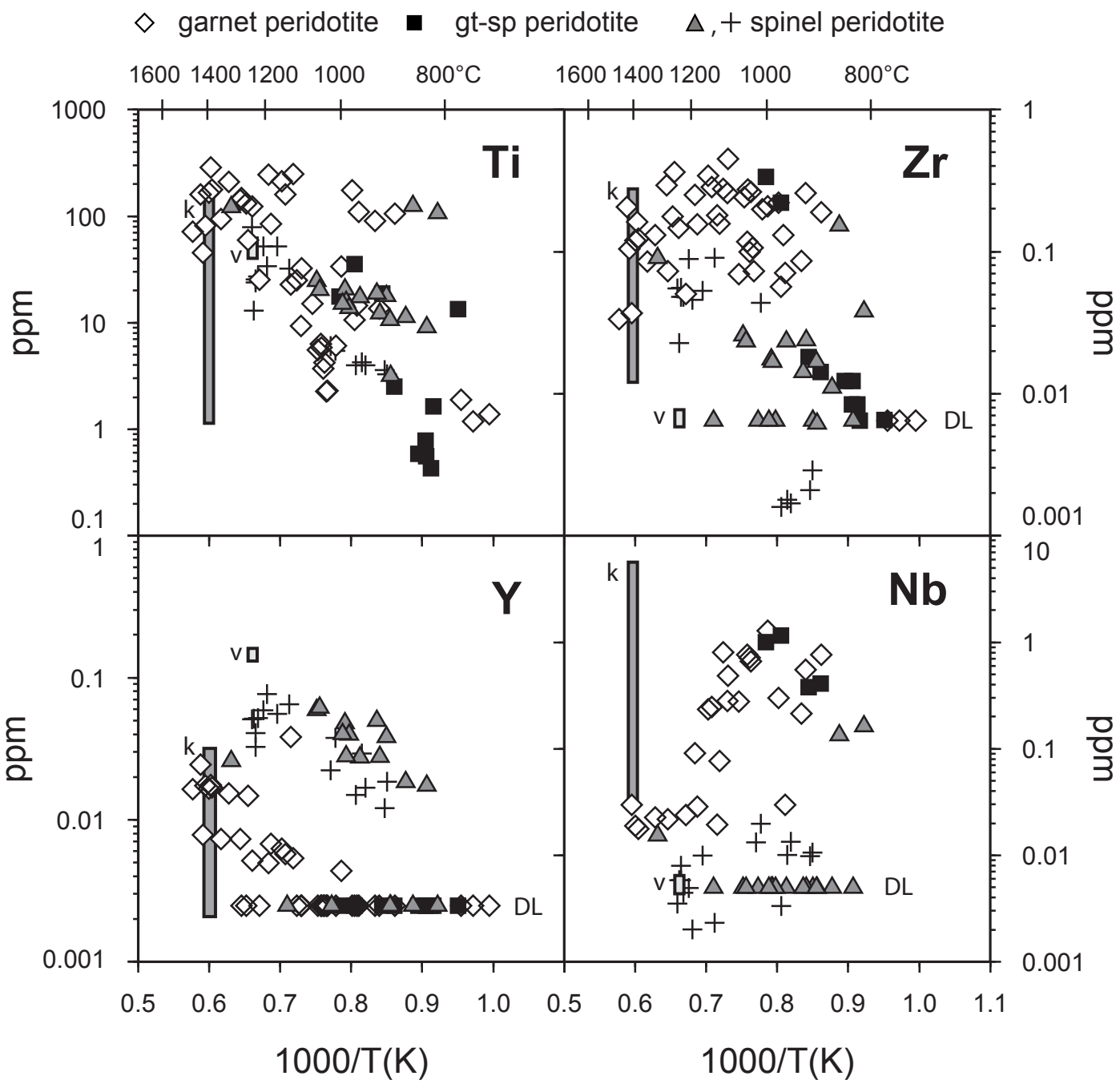


Fig. 5 De Hoog (submitted to Chem Geol)

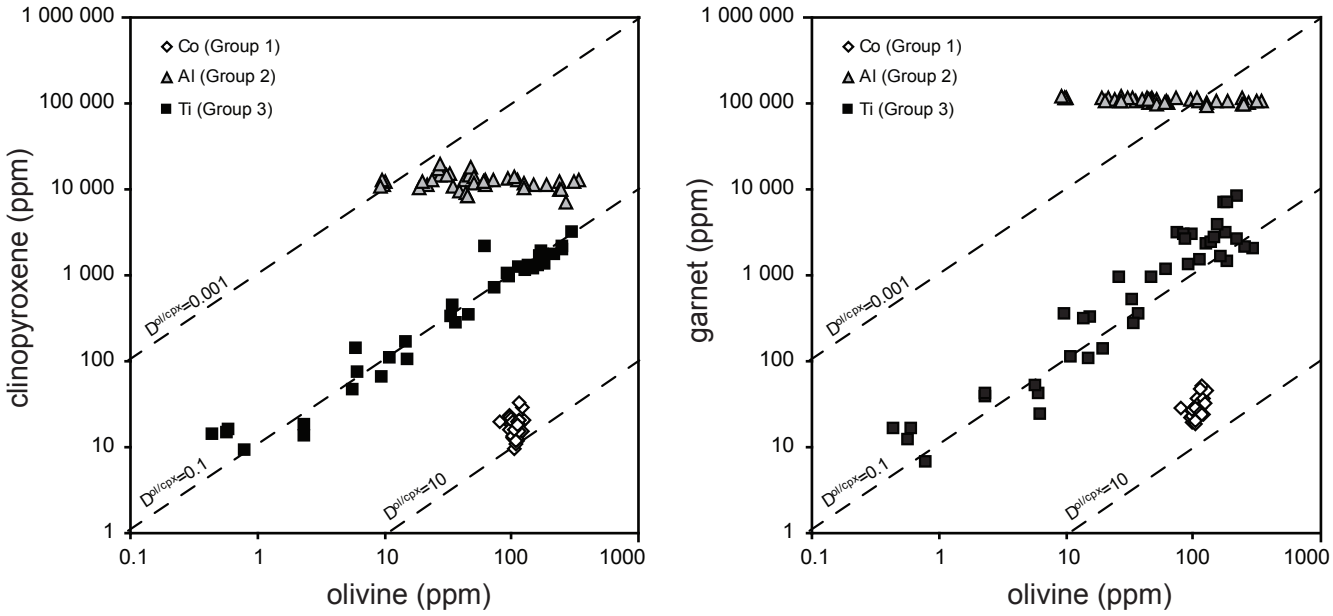


Fig. 6. De Hoog et al. (submitted to Chem Geol)

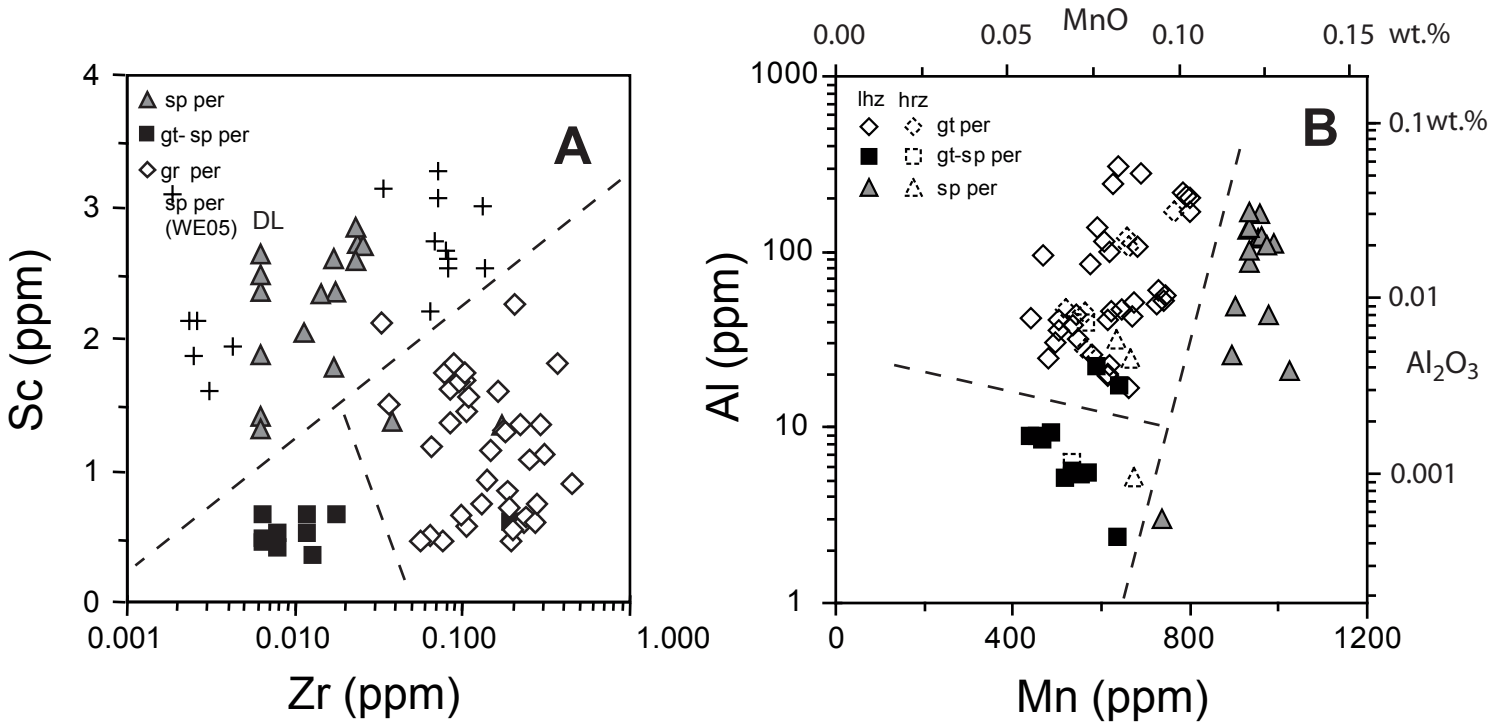


Fig. 7 De Hoog (submitted to Chem Geol)

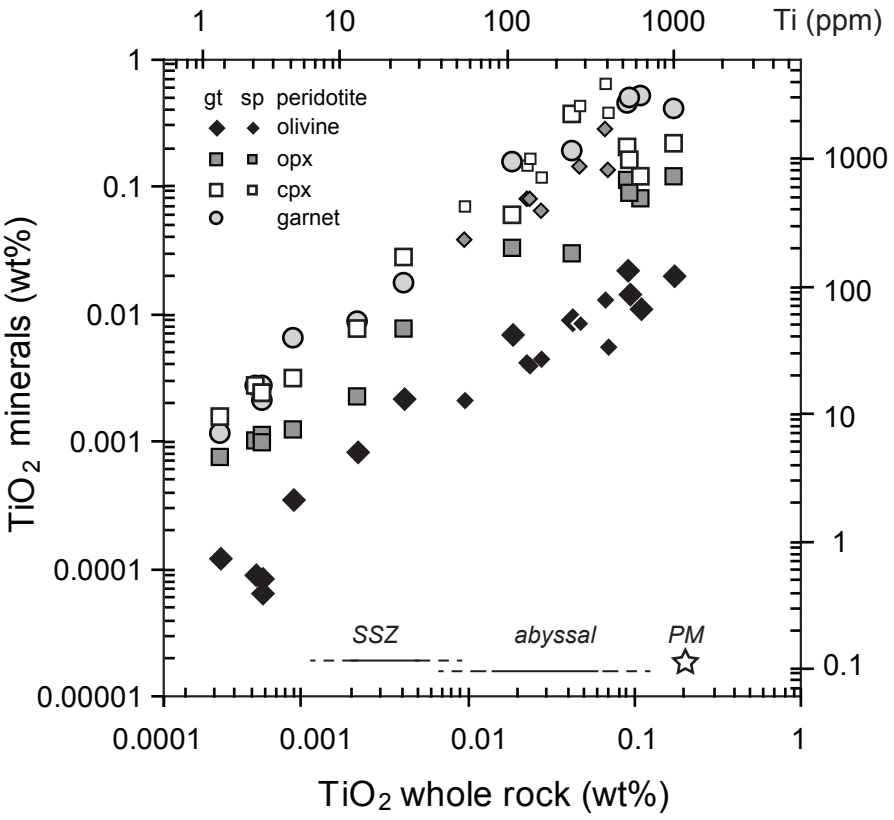


Fig. 8. De Hoog (submitted to Chem Geol)

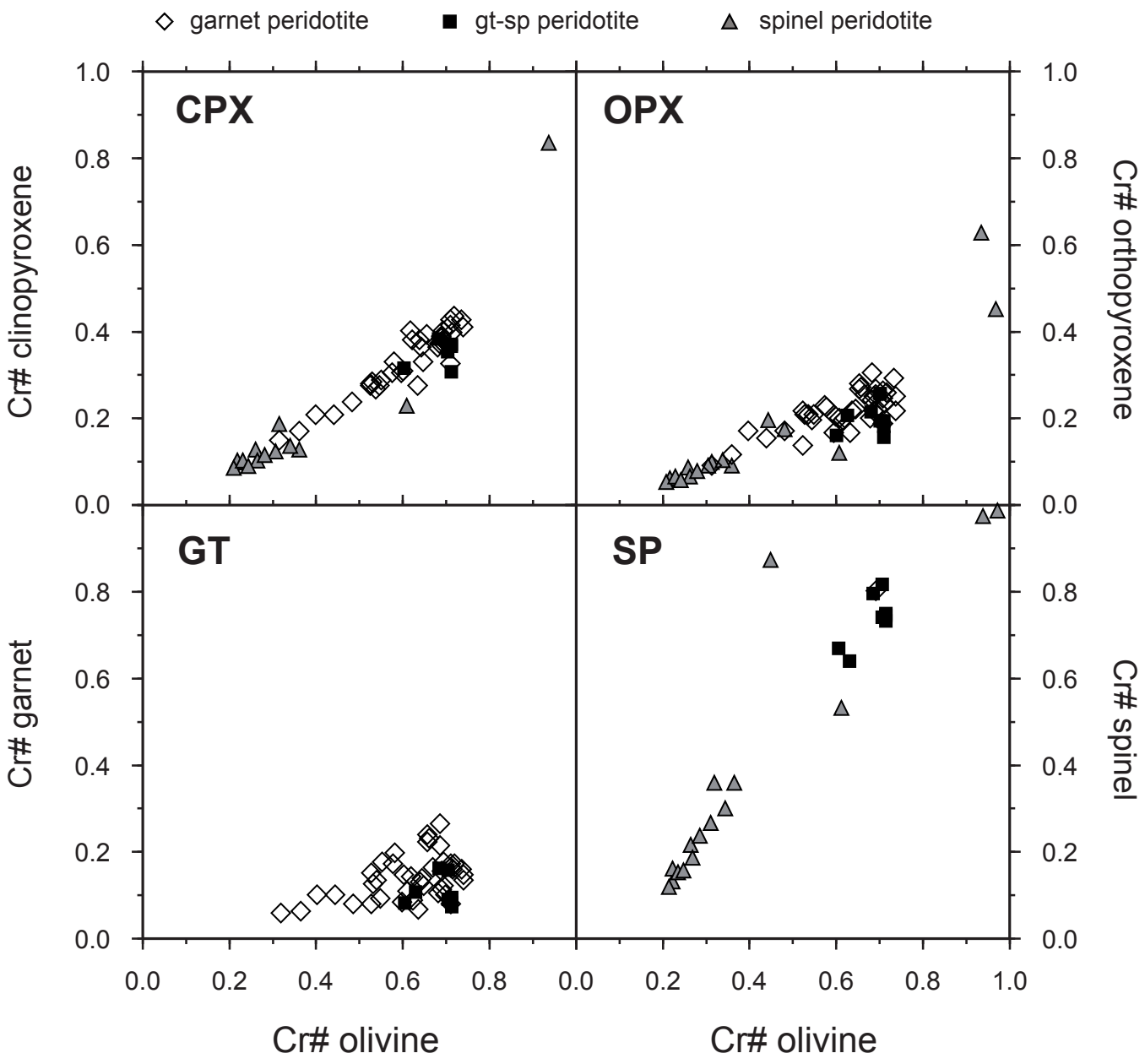


Fig. 9 De Hoog (submitted to Chem Geol)

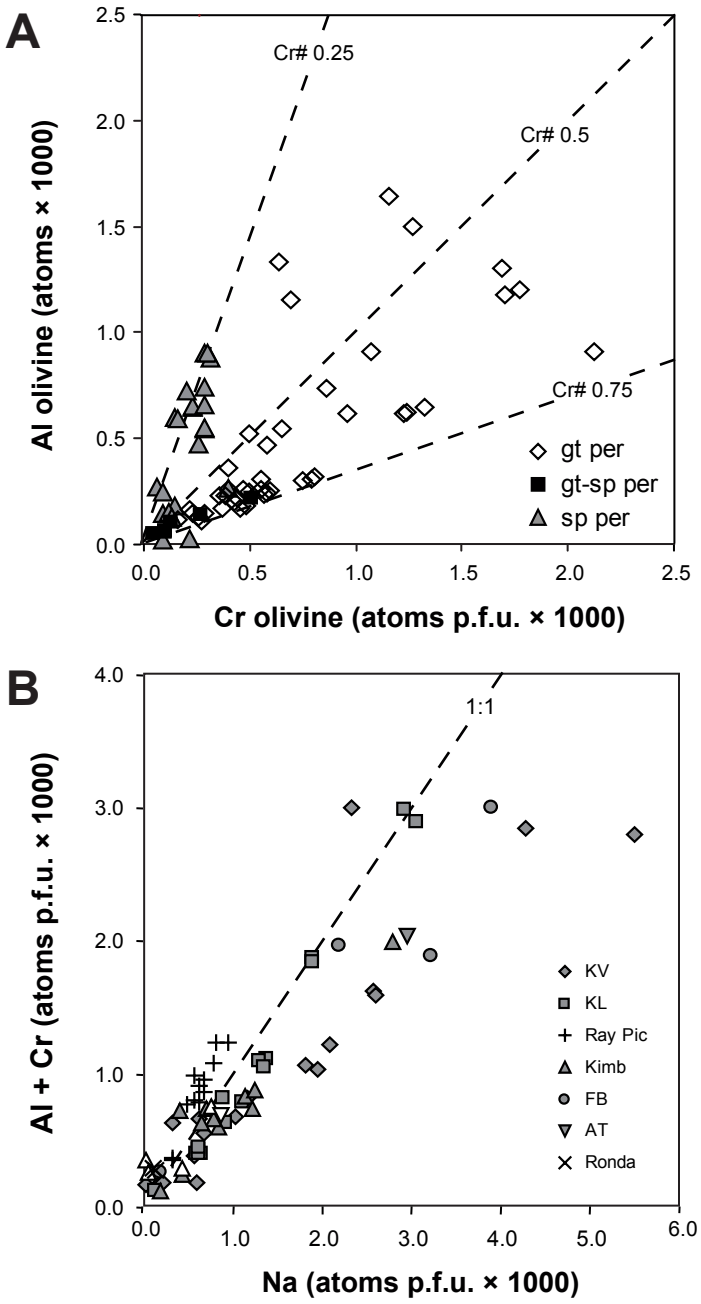


Figure 10. De Hoog (submitted to Chem Geol)

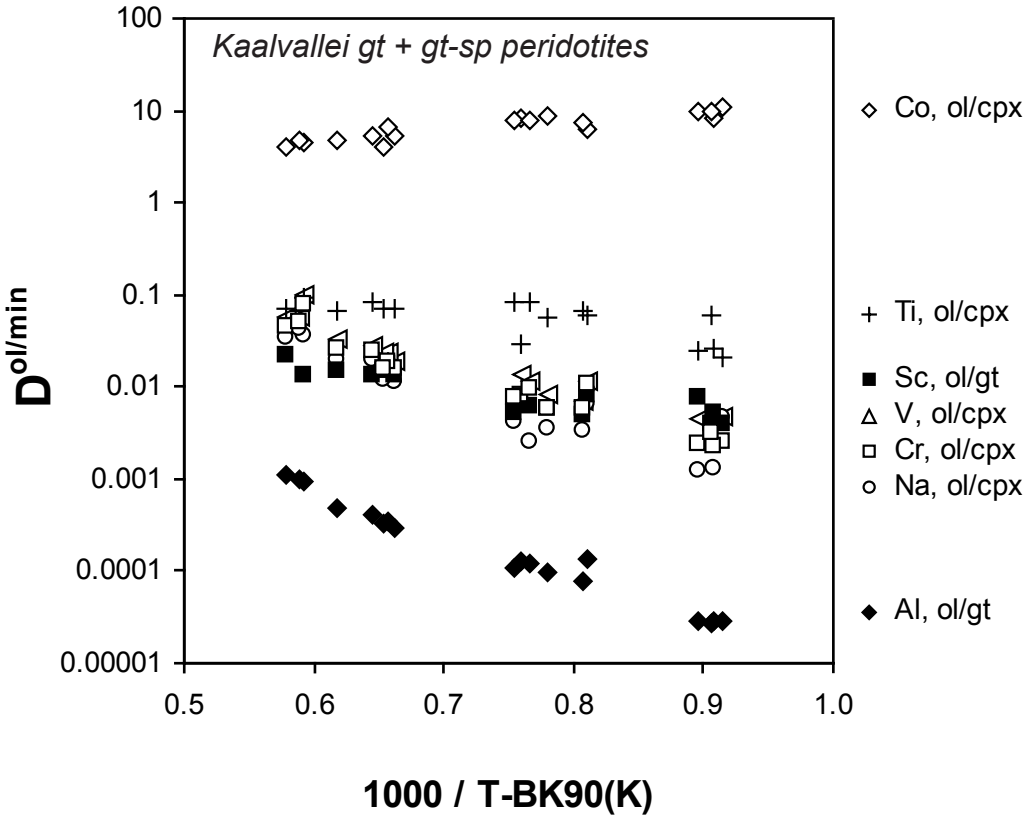


Figure 11. De hoog (submitted to Chem Geol)

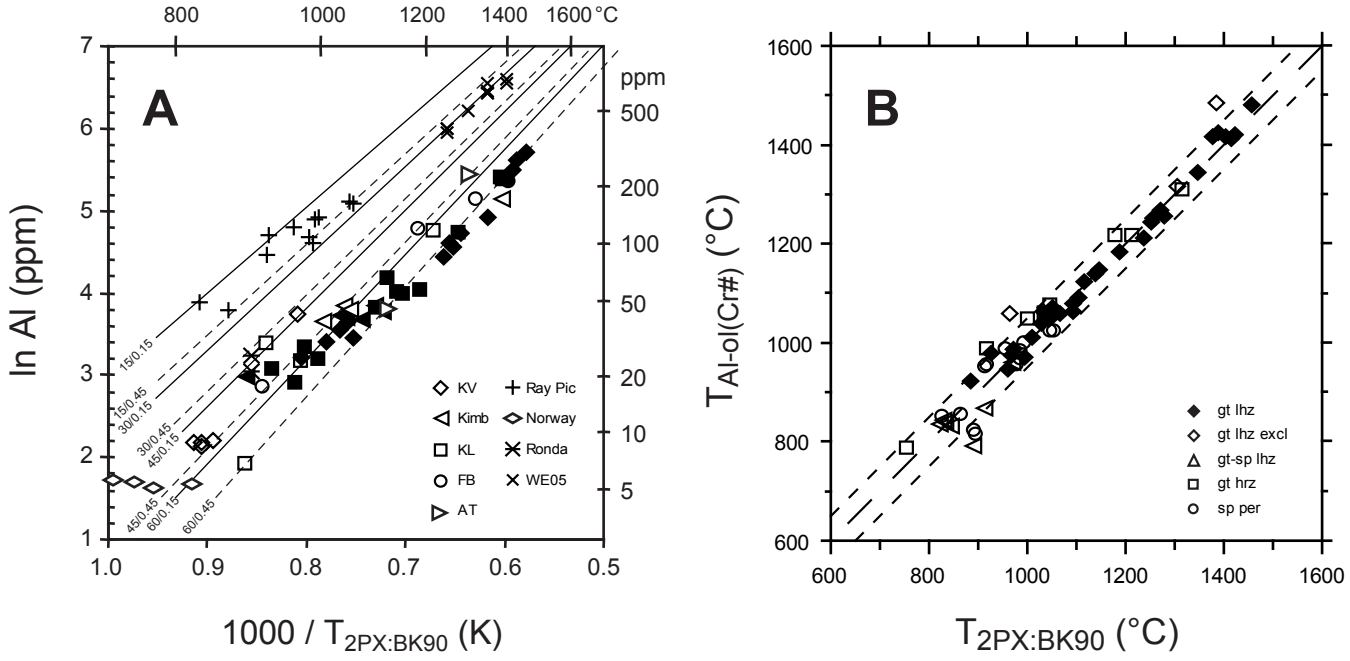


Figure 12. De Hoog (submitted to Chem Geol)